Petroleum Science 23 (2026) 103–126

Contents lists available at ScienceDirect

Petroleum Science

journal homepage: www.keaipublishing.com/en/journals/petroleum-science

Original Paper

Impacts of Himalayan tectonism on Eocene gas shale and its pore structure within the Lesser Himalayas, Nepal: Insights for shale gas accumulation and preservation

Kumar Khadka [a,b,c,d,e,1], Si-Jie Han [b,c,1,*], Shu-Xun Sang [a,b,c,**], Jun-Jie He [a,b,c], Upendra Baral [e,f], Saunak Bhandari [d,e], Debashish Mondal [a,b,c], Xiao-Zhi Zhou [b,c], Shi-Qi Liu [b,c]

[a] School of Resources and Earth Science, China University of Mining and Technology, Xuzhou, 221008, Jiangsu, China
[b] Jiangsu Key Laboratory of Coal-based Greenhouse Gas Control and Utilization, China University of Mining and Technology, Xuzhou, 221008, Jiangsu, China
[c] Carbon Neutrality Institute, China University of Mining and Technology, Xuzhou, 221008, Jiangsu, China
[d] Department of Mines and Geology, Government of Nepal, Kathmandu, 44600, Nepal
[e] Institute of Fundamental Research and Studies (InFeRS), Kathmandu, 44600, Nepal
[f] State Key Laboratory of Tibetan Plateau Earth System Science, Resources and Environment, Institute of Tibetan Plateau Research, Chinese Academy of Sciences, Beijing, 100101, China

ARTICLE INFO

Article history:
Received 10 May 2024
Received in revised form
6 September 2025
Accepted 15 September 2025
Available online 20 September 2025

Edited by Jie Hao and Xi Zhang

Keywords:
Gas shale
Eocene foreland basin
Pore structure
Tectonic deformation
Himalayan tectonics
Gas preservation

ABSTRACT

This study investigates the complex relationship between organic matter (OM), tectonic deformation, and pore structure development in Eocene Bhainskati shale within the Lesser Himalayan foreland basin, Nepal, to assess its implications for shale gas accumulation and preservation. We hypothesize that tectonic deformation and variations in organic matter have a significant impact on pore size distribution, connectivity, and gas retention, thereby influencing shale gas potential. We characterized pore types and quantified pore size distributions using scanning electron microscopy (SEM), mercury intrusion capillary pressure (MICP) techniques, and low-pressure gas adsorption methods. Our findings indicate a predominance of mesopores (1–10 nm range, with a notable peak at 4 nm), suggesting substantial contributions to surface area from micropores and fine mesopores. Thermal maturity negatively impacts porosity and surface area. At the same time, tectonic activity enhances microfracture development, increasing permeability and gas transport, particularly in the Surkhet area, which exhibits higher pore volume and specific surface area than the Tansen area. Tectonic forces shift the shale from brittle to ductile behavior, altering pore connectivity. Himalayan tectonic forces significantly influence shale structure, pore sizes, gas preservation, and migration, enhancing gas adsorption by increasing surface area but posing challenges due to potential gas escape along faults and folds. Understanding the impact of tectonic activity on shale deformation in similar basins within the Himalayas and the adjacent region is vital for assessing shale gas potential and optimizing exploration strategies in tectonically active Nepal Himalayan regions. This study highlights the dual role of tectonics in both promoting and complicating the formation, accumulation, and preservation of shale gas reservoirs, offering critical insights for future exploration efforts.

* Corresponding author.
** Corresponding author.
E-mail addresses: hsj_cumt@126.com (S.-J. Han), shuxunsang@163.com (S.-X. Sang).
Peer review under the responsibility of China University of Petroleum (Beijing).
[1] These authors contributed equally to this work.

https://doi.org/10.1016/j.petsci.2025.09.026

1. Introduction

The global importance of unconventional natural gas, particularly shale gas, has prompted extensive research into understanding the intricate pore structure of shale reservoirs, which significantly influences gas distribution and preservation (Xu et al., 2020). Shale constitutes various pore types, sizes, and distributions that influence hydrocarbon distribution (Slatt and O'Brien, 2011). Shale gas is stored mainly in organic matter within a shale matrix, existing in compressed free gas, adsorbed gas, and dissolved gas forms (Chalmers et al., 2012; Curtis, 2002; Xiong et al., 2017). The pore structure of shale significantly influences its petrophysical properties, governing hydrocarbon accumulation, preservation, and transmission (Chen et al., 2021; Ghanizadeh et al., 2015). Characterizing pore types, structure, development, and influencing factors is crucial for shale reservoir research (Josh et al., 2012; Medina-Rodriguez and Alvarado, 2021). Comprehensive analyses of pore systems through methods such as MICP and low-pressure gas adsorption (LPGA) provide quantitative assessments of parameters like porosity, pore size distribution (PSD), surface area (SA), and pore volume (PV) (Ma et al., 2022; Mastalerz et al., 2018; Ross and Marc Bustin, 2009; Sun et al., 2020; Wang et al., 2024). Nitrogen sorption isotherms are widely employed to evaluate surface area, pore size, and connectivity in nanoporous media, utilizing approaches like the Brunauer-Emmett-Teller (BET) theory and the Barrett-Joyner-Halenda (BJH) method (Sing, 2001; Xu and Prodanović, 2018). Image analysis methods through transmission/scanning electron microscopy (TEM/SEM) and other high-resolution microscopes can be used to observe shale geometry, microstructure characterization, and pore size (Bai et al., 2024; Qian et al., 2022). The formation and evolution of shale pore structures are influenced by various geological factors, including mineral composition, total organic carbon (TOC), OM type and chemical composition, diagenesis, and thermal maturity (Chalmers et al., 2012; Clarkson et al., 2013; Curtis et al., 2012; Liang et al., 2017; Ross and Marc Bustin, 2009). Shale is rich in organic matter, which may deform at low pressure and temperatures, and tectonic stresses can significantly influence its pore structure and composition (Liang et al., 2017). Natural fractures in shale gas reservoirs are influenced by tectonic stress and rock composition, with shale quality and preservation crucial for gas generation, especially near faults and thrusts (Shang et al., 2021). Mechanical deformation primarily impacts the development and evolution of the pore structure and increases the connectivity of pore networks during the tectonic process. The development of InterP pores, micro-channels, and micro-fractures is intimately associated with the pore structure of the shale, which varies significantly depending on the tectonic stress (Zhu et al., 2018).

Tectonic movements during the Himalayan orogeny enhanced shale gas retention by shaping pore structures, increasing connectivity, and influencing fracture networks. Late and low-intensity tectonic uplift aids in gas preservation, affecting shale fractures and overpressure (Chen et al., 2024; Gao et al., 2023; Guo, 2016). Intense Himalayan tectonic activity complicated the geological setting of organic-rich shales, impacting their gas retention through brittle and ductile deformations in southern China (Sun et al., 2021; Sun et al., 2023; W. Sun et al., 2020; Zeng et al., 2023). Tectonic deformations affect the source and reservoir rocks through brittle deformation, ductile deformation, or a mixture of the two according to their mineralogical composition. Hydrocarbon reservoirs with dual medium pore fracture systems serve as shale gas preservation and transportation, which could be affected by the tectonic moments by reopening the existing microfractures (Feng et al., 2022). Structural deformation and tectonic stress impact shale's pore surface area and adsorption capacity but do not affect shale mineral composition, maturity, porosity, and total pore volume (Liang et al., 2017). The meso-macropores are more significant than the difference in the microporous volume, implying that geological tectonism substantially impacts the meso-macropores more than the shale samples (Sun et al., 2023). The Himalayan thrust belt in Nepal is characterized by significant tectonic activity and crustal shortening, manifested through key structural features such as the frontal imbricate zone, synformal klippen of Greater Himalayan Sequence rocks, and the Lesser Himalayan duplex (DeCelles et al., 2020). The shale from the tectonic structures interacts with the Proterozoic low-grade metasedimentary rocks from the Lesser Himalayan Sequence, juxtaposed against the Eocene-Miocene foreland deposit and the Siwalik Group due to the Main Boundary Thrust (MBT) (DeCelles et al., 2020). Such tectonic movements in the Himalayas have influenced the preservation and enrichment of hydrocarbons in the Eocene shale, with distinct effects on different hydrocarbons preserved in strata (Singh et al., 2016). Despite some research on Eocene shale in the Himalayas focusing on source potential and reservoir characterization (Craig et al., 2018; Hafiz et al., 2022; Khadka et al., 2024, 2025; Li et al., 2022; Mani et al., 2014; Ping et al., 2021; Wang et al., 2022, 2023; Yang et al., 2021), there remains a gap in understanding the pore characteristics of Himalayan foreland Eocene shale.

This research explores gas adsorption and preservation of organic black shale, thermally mature and ductile within the tectonically active Eocene foreland, Lesser Himalayas, aiming to understand how significant tectonic activity affects shale pore structures, porosity, and permeability, impacting shale gas potential. This study involves characterizing pore network properties, quantifying matrix pores and fractures, and analyzing geological factors' effects on porosity, pore size distribution, and permeability of the Eocene foreland shales within the Lesser Himalayas in the Tansen and Surkhet regions of Nepal (Fig. 1) through imaging techniques and fluid intrusion methods. This research aims to unravel how TOC, mineralogy, thermal maturity, and porosity of Eocene shale interplay with Himalayan tectonics, impacting gas accumulation and preservation. Finally, this study conducts a comparative analysis of the Bhainskati Formation shale in the tectonically active Nepal Himalayas with analogous formations, including the Subathu Formation (India), the Patala Formation (Pakistan), and shales in the Sichuan and Guizhou regions (China), to investigate the influence of structural deformation on pore structure and its implications for shale gas accumulation and preservation.

2. Geology

The Lesser Himalayan sequence comprises a diverse range of formations spanning from Precambrian-Proterozoic rocks to Permian to Cretaceous layers, including the Gondwana sequence and Eocene to lower Miocene foreland deposits (De Celles et al., 2004). Several peripheral foreland basins were created in response to the initial India–Asia collision between the Late Paleocene and Early Eocene. The Amile, Bhainskati, and Dumri Formations are associated with the Surkhet/Tansen Group, which extends from the Late Cretaceous to the Miocene age. Within this sequence, the Eocene foreland deposit Bhainskati Formation stands out, ranging from 90 to 150 m thick. It is characterized by gray to black shales abundant in foraminifera, marine calcareous fossils, coalified wood fragments, and carbonaceous flakes, often exhibiting signs of bioturbation (Sakai, 1983). The thin and sporadic coal seams and laminated black shale were deposited during the early transgressive phases in the Eocene, predating the collision of the Indian and Eurasian plates (Singh et al., 2016). The

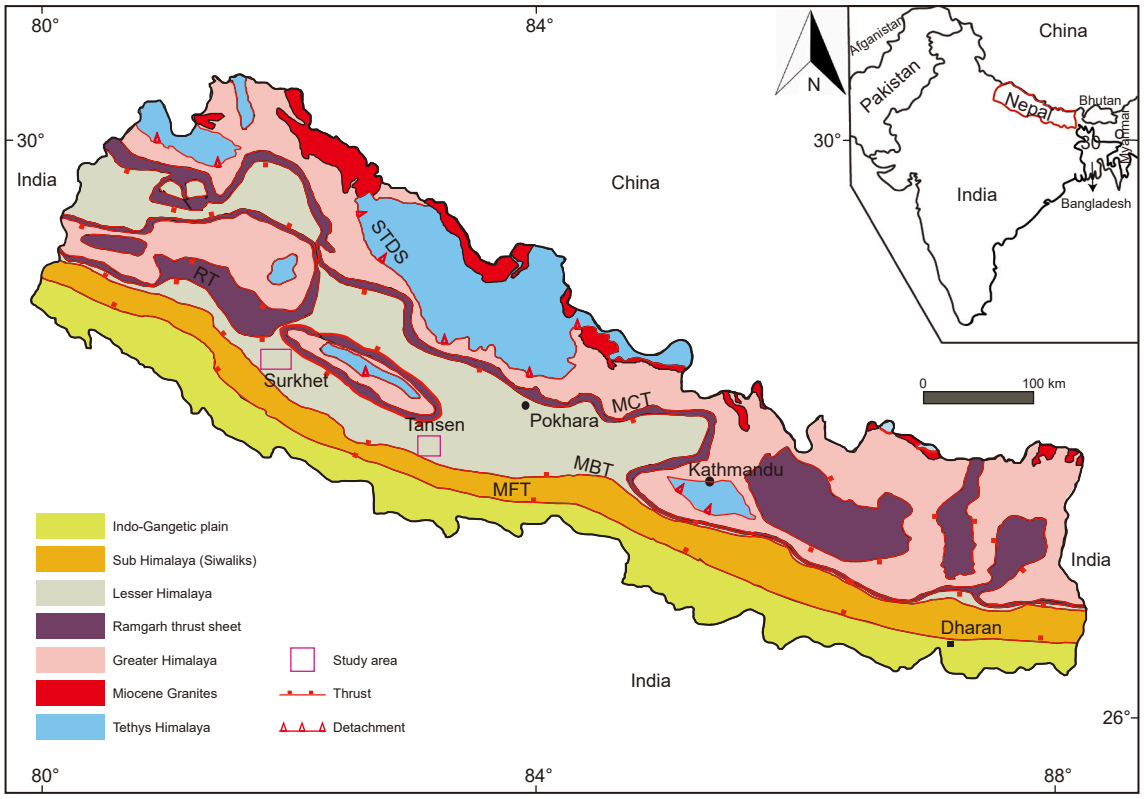

Fig. 1. Generalized geological map of Nepal with the study area modified after DeCelles et al. (2004).

Bhainskati Formation lies above the Amile Formation, and the Dumri Formation is overlained to it (Fig. 2).

The intricate tectonic deformations found in the Tansen and Surkhet areas' foreland basins within the Lesser Himalayas result from multiple cycles of tectonic activity. Following the significant hydrocarbon generation period, the Main Central Thrust (MCT) caused the Greater Himalaya to thrust over the Lesser Himalaya, and the MBT caused the Lesser Himalaya to thrust over the younger sedimentary foreland strata. This evolution unfolds through multiple stages, including the Indian-Asian plate collision around 55–50 million years ago, initiating sediment deposition in the shallow marine Tethys sea from both south and north highlands (Fig. 3(a)–(c)) and leading to significant geological transformations (DeCelles et al., 2004). Various thrusts sandwich the Lesser Himalayan imbricates, including the Lakharpata, Gondwana, and Eocene-Miocene foreland units. The MCT and Ramgarh fault (RT) were active during the early to middle Miocene period. The RT extends southward in the footwall, reaching Paleocene–Lower Miocene rocks from the northern exposures of the Lakharpata Group (DeCelles et al., 2020). The Lesser Himalayan duplex expanded primarily between 11 and 5 Ma, whereas the MBT started to operate after 5 Ma (Fig. 3(d)–(f)) and is probably still active in some locations (DeCelles et al., 2004; Robinson et al., 2001). These tectonic movements have significantly affected the underlying strata, including increased erosion, basal friction, and changes in lithological composition and fluid pressure within the wedge (DeCelles et al., 2004, 2020). In the Tansen area, the geological landscape is characterized by the rocks of the Tansen Group, forming an approximately doubly plunging synclinorium, displaying moderately folded structures, mainly influenced by longitudinal faults associated with the overthrust of the Palpa Klippe (Sakai, 1983). This Klippe interfaces predominantly with the Amile Formation and also with the Bhainskati and Dumri Formations towards its southeastern and eastern edges (Fig. 2(a)). Consequently, the resultant faults and folds have notably influenced the Bhainskati Formation, leading to alterations in pore structures and shale deformation, impacting the origin and preservation of shale gas resources (DeCelles et al., 1998).

3. Samples and methods

Three fresh outcrop samples from the Tansen (Fig. 2(a)) and Surkhet (Fig. 2(b)) areas were meticulously collected, focusing on the Eocene foreland Bhainskati Formation. Minimizing surface weathering and degassing, which can significantly alter original petrophysical properties, we collect samples exclusively from fresh, unweathered exposures (road cuts and river cuttings) and mechanically remove the weathered rind to access the pristine rock interior. Color, organic matter content, texture, and morphological characteristics were carefully considered to study pore structure, mineralogy, and tectonic influences. The shale samples are dark gray to black and exhibit a platy structure. Furthermore, two samples from the Gondwana Sisne Formation in the Tansen area were taken for comparative study with the Eocene shale.

3.1. X-ray diffraction and organic geochemistry

We meticulously tested six fresh outcrop shale samples from the Eocene Bhainskati Formation of the Tansen and Surkhet areas for their mineralogical and geochemical assessments. Additionally, we examined two samples from the Gondwana Group to conduct a comparative study with the Eocene samples. X'Pert Pro MPD DY3794 was used for X-ray diffraction (XRD) analysis in the Laboratory of Coal Geology Bureau of Guizhou Province, China, to examine the bulk mineralogical composition of the samples.

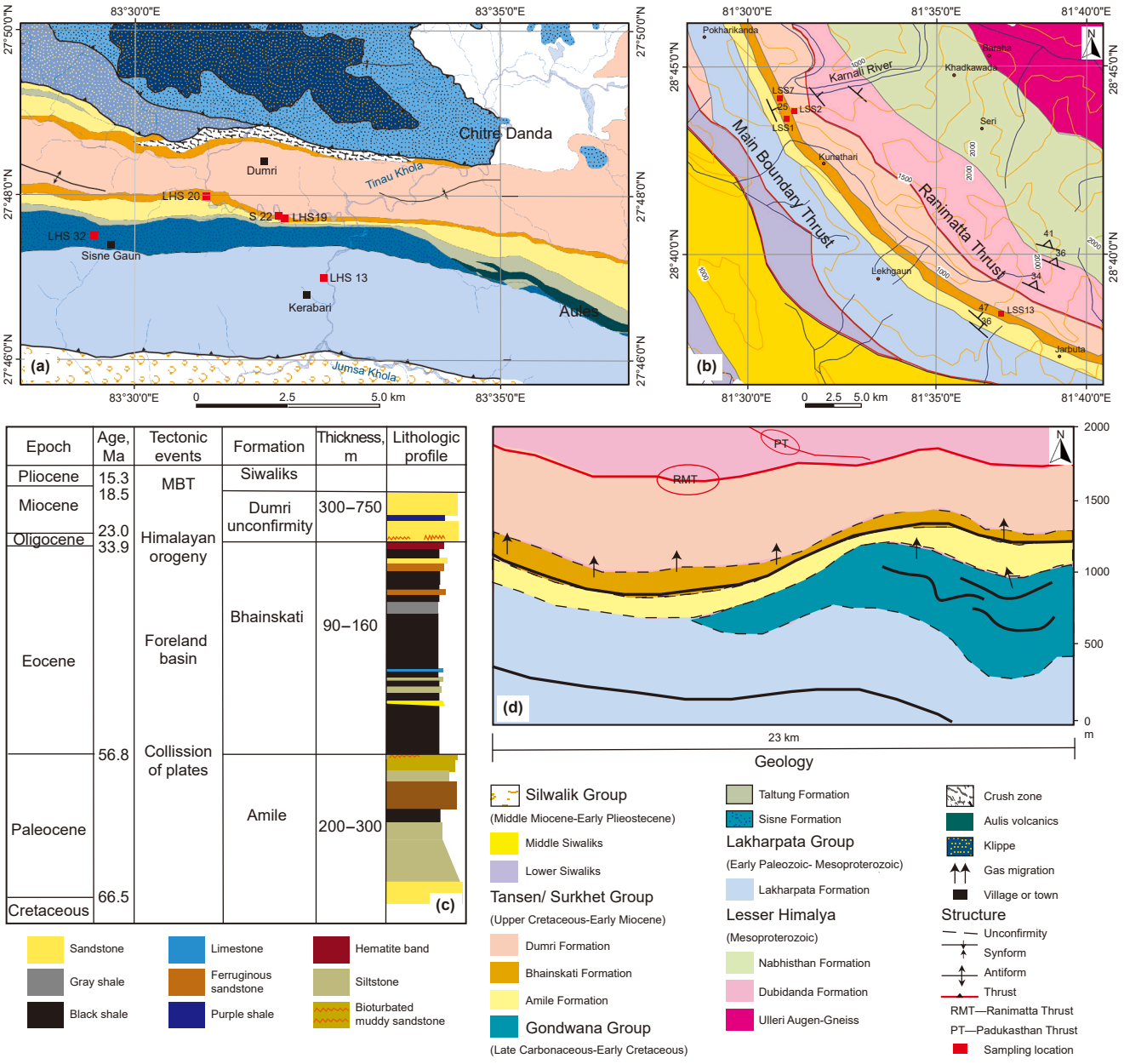

Fig. 2. (**a**) Geological map with sample location of Tansen, modified after Sakai (1983), Dhital (2015), (**b**) geological map of the Surkhet area with sampling location modified after DeCelles et al. (2020), (**c**) the lithological columnar section of foreland deposits in Tansen is modified after Sakai (1983), and (**d**) the Geological profile of the Surkhet area modified after Yang et al. (2021).

Before the XRD analysis, we ground all samples into a powder with an average particle size of less than 300 mesh. After that, about 10 g of powder shale samples were mixed with ethanol, hand-ground, and then smear-mounted on glass slides for XRD analysis. The detection method followed the X-ray diffraction analysis method for clay minerals and common non-clay minerals in sedimentary rocks, SY/T 5163-2018. We utilized the Infrared sulfur analyzer (LECO CS-230) to test the TOC content. Rock-Eval VII instruments were used for pyrolysis parameters at Wuhan Xinshengji Technology Co., Ltd, China, following the GB/T 18602-2012 "Rock Pyrolysis Analysis" guidelines. Vitrinite reflectance is determined by the Polarizing microscope Scope A1, following the SY/T5124-2012 standard method at the Laboratory of Coal Geology Bureau of Guizhou Province.

3.2. Field emission-scanning electron microscopy (FE-SEM)

Scanning Electron microscope conditions included room temperature (17–25 °C), humidity <65%, circulating water cooler temperature of 20 ± 2 °C, air compressor output pressure of 5–6 bar, high purity nitrogen (99.999%), gun vacuum $<5 \times 10^{-9}$ mBar, system vacuum $<5 \times 10^{-5}$ mBar, high voltage (EHT) of 12–18 kV, and working distance (WD) of 8–10 mm was used for SEM analysis. A German ZEISS SIGMA field emission scanning electron microscope, combined with the UK OXFORD X-Max20 energy spectrum, was used to analyze shale pore-fracture systems at the Geology and Mineral Resources Design Institute of Jiangsu Province, China. These images facilitated the examination of reservoir pore structures and microfractures, analyzing

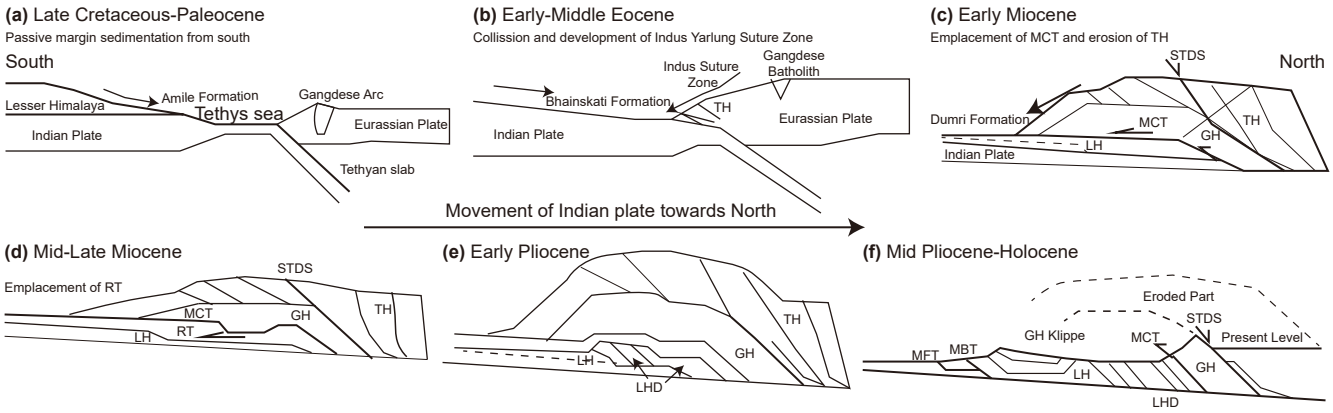

Fig. 3. Himalayan foreland deposition with sediment provenance model diagram ((**a**)–(**c**) modified after DeCelles et al. (2004) and ((**d**)–(**f**)) Tectonic model diagram describing the formation of the Lesser Himalayan duplex LHD, Ramgarh Thrust sheet RT, Main Central Thrust sheet MCT, Main Boundary Thrust MBT, and Main Frontal Thrust MFT sheet in Nepal Himalaya (modified from Robinson et al. (2006)). Dashed lines in (f) mark the positions of stratigraphic units before erosion. Abbreviations: TH-Tibetan Himalayan; GH-Greater Himalayan; LH-Lesser Himalayan; STDS-South Tibetan Detachment system.

characteristics such as size, shape, connectivity, and surface morphology. SEM provides high magnification, resolution, sharpness, and stereoscopic images, enabling observation and description of pores at different levels and of various genetic types.

3.3. Mercury intrusion capillary pressure (MICP) analysis

The Micromeritics Autopore IV 9500 V 1.09 instrument was used to conduct MICP experiments with pressures up to 60,000 psi after drying samples at 70–80 °C for 12 h. MICP primarily analyzes macropores in shale samples, with mercury filling occurring from 0.0036 to 387.4574 MPa. Pore diameters ranging from 349 to 3.2 nm were calculated using the Washburn equation, employing a surface tension of 0.48 N/m and a contact angle of 130°. Pore size distributions were quantified at the Laboratory of Guizhou Coal Field Geological Bureau, Guizhou, China. The shale samples underwent rigorous testing for porosity, permeability, pore diameter, rock density, intrusion pore volume, and pore area.

3.4. Low-pressure gas adsorption (LPGA) analysis

Gas adsorption methods encompass nitrogen adsorption (N_2) and carbon dioxide (CO_2) adsorption, which are utilized to characterize nano-scale open pores based on the shape of the adsorption-desorption curve (Liu et al., 2015). N_2 adsorption assesses mesopore distribution (1–200 nm) in shale, while CO_2 adsorption detects micropore characteristics (<2 nm) due to its small diameter and strong adsorption potential (Yin et al., 2019). Tests utilized a Nova 4200e gas adsorption instrument (Quantachrome, America), measuring specific surface areas (SSA), PV, and pore diameters (0.35 nm–400 nm). High-purity liquid nitrogen was employed as the adsorbate in the low-pressure nitrogen adsorption analysis, which was carried out at 77.35 K with a relative pressure (P/P_0, where P is the current pressure and P_0 is the saturated vapor pressure of nitrogen at −77 K) ranging from 0.005 to 0.995. The adsorbate in the low-pressure CO_2 adsorption experiment was carbon dioxide, and the experiment was conducted at 273.15 K with a P/P_0 range of 0.00003–0.035 at the Laboratory of China University of Mining and Technology, Xuzhou, China. PSD, SSA, and PV were determined using multi-point Brunauer-Emmett-Teller (BET) and Langmuir analysis, and the CO_2 adsorption provided the BJH microporous data (Chalmers et al., 2012).

Integration of MICP and LPGA evaluated the shale reservoir's pore size distribution. The mercury first enters the macropore under low pressure, then the mesopore and micropore under high pressure. High pressure may cause pore deformation. Therefore, the MICP experiment is the most accurate representation of macropore distribution, and CO_2 is first filled in the micropore and then adsorbed in the mesopore. However, because the saturated vapor pressure of CO_2 in the ice water bath condition is extremely high, it can more easily enter the micropore than N_2. Hence, CO_2 adsorption experiments are more suitable for characterizing the micropore, and N_2 adsorption experiments are ideal for describing the mesopore. N_2 and CO_2 adsorption-desorption curves characterize pore structure type, volume, and specific surface area of mesopores and micropores.

4. Results

4.1. Organic geochemistry and physical properties of shale

The results of total organic content, thermal maturity, and T_{max} are summarized in Table 1. The experimental findings of the analyzed shales indicate the average TOC of shale samples extends from 0.63% to 1.56% with an average of 1.25%. The T_{max} values range from 480 to 507 °C based on the Rock-Eval data, and the thermal maturity (R_o) values vary from 1.05% to 2.955% (Table 1), revealing that the samples are thermally over-matured within the dry gas window. Based on the results of TOC and Rock-Eval pyrolysis data, the organic matter is mainly type III kerogens.

The bulk mineralogical composition analysis done by XRD is listed in Table 2. The shale is dominated by clay minerals (illite) and quartz (Table 2). The Bhainskati shales comprise quartz (22.33%–40.55%) and clay (48.51%–62.54%). Among the clay minerals, illite has an average of 73.51%, followed by chlorite (8%–19%) and kaolinite (5%–11%) as significant clay minerals (Table 2). Pyrite is observed only in sample F304 with 1.87%. The brittleness index (BI) is widely used to characterize the fracability of rock masses and is expressed as (Jarvie et al., 2007):

$$\mathrm{BI} = \frac{Q}{Q + \mathrm{Ca} + \mathrm{Cl}} \quad (1)$$

where Q is the weight content of quartz minerals, Ca is the weight content of carbonate minerals, and Cl is the weight of clay

Table 1
R_o, TOC, and other pyrolysis data of the shale samples.

Sample ID		Location			Formation/Group	TOC	R_o	T_{max}
		Longitude	Latitude	Area				
F298	LHS19	83.541	27.796			0.71	1.626	481
F304	S22	83.533	27.796	Tansen	Bhainskati	0.84	2.955	480
F280	LHS20	83.516	27.800			1.56	1.721	501
F301	LSS1	81.513	28.738			1.49	1.515	500
F302	LSS13	81.615	28.642	Surkhet	Bhainskati	0.93	2.495	507
F303	LSS7	81.518	28.739			0.63	1.055	480
F300	LHS32	83.491	27.792	Tansen	Gondwana	0.75	2.000	480

Longitude-Latitude, degree decimal; R_o, vitrinite reflectance, %; T_{max}, °C; TOC, %.

minerals. BI of shale in the Eocene Bhainskati Formation is within the ductile zone except for one sample, LHS20, shown in the brittle-ductile transition zone (Table 2). Calcite is observed in the Eocene and Gondwana shale samples within the range (2.23–27.29) wt.%, but not in all samples. The Gondwana shale sample is also within the same clay and quartz content range, but consists of plagioclase of (13.76–19.65) wt.% (Fig. 4).

4.2. SEM image analysis

The internal pore structures of the Eocene shale samples were examined using FE-SEM imaging, as depicted in Fig. 5. Shale pores are categorized into matrix pores and fractures. The major pore types observed in the analyzed shale samples are interparticle (InterP), intraparticle (IntraP), and OM. Matrix pores consist of InterP pores between clay particles or quartz, IntraP pores within quartz, clay, and OM pores within organic matter (Loucks et al., 2012). InterP pores range from tens to hundreds of nanometers and come in elongated, rounded, angular, and slit-like shapes (Fig. 5(a)–(c), (e)). IntraP pores are observed within quartz, clay, and organic matter and can appear as dissolution pores (Fig. 5(c)–(f)). OM pores are smaller and round or oval in shape. InterP pores are interconnected by microfractures, which are parallel to each other and the bedding plane (Fig. 5(a)). These features, along with fractures, are visible in the FE-SEM images of Bhainsekati shales (Fig. 5). Fractures are found within splits of flake clay minerals or at the edges of brittle minerals, often exhibiting a jagged or irregular border or a zigzag shape.

4.3. MICP analysis

MICP analysis shows that representative shale samples from the Eocene Bhainskati Formation and the Gondwana Sisne Formation ranged in density from 2.39 to 2.685 g/cm^3, averaging 2.51 g/cm^3. Effective porosity varied between 2.40% and 8.41%; dense shale typically shows low permeability, in the range of 0.925–9.01 mD (Table 3).

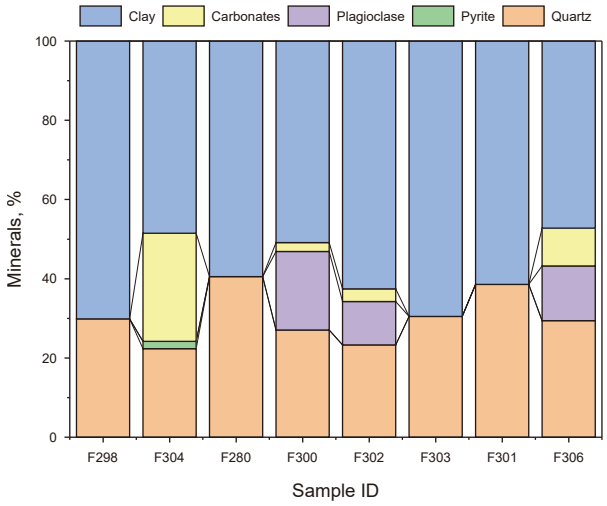

Fig. 4. Mineralogical composition of shale samples of the Eocene Bhainskati and Gondwana Sisne Formation.

Similarly, the total intrusion pore volume ranges from 0.009 to 0.035 cm^3/g. The total pore area of shale from Surkhet is the highest at 5.361–9.791 m^2/g, and that in the Tansen area is 1.148–7.243 m^2/g. The average pore diameter ranges between 14.3 nm and 20 nm in the Surkhet area and 19.2–40.6 nm in the Tansen area. Fig. 6(a) and (b) illustrates the pore size distributions of seven shale samples analyzed using MICP. Shale pores range from about 5 to 100 μm, with nanopores (<300 nm) comprising a significant portion and pore-microfractures (>1000 nm) making up a smaller portion. The pore network, governed by primary pore conservation and secondary pore development, determines the reservoir quality. Fig. 6 presents the diverse PSD curves of all bulk shale samples, exhibiting distinct peak patterns. All the peaks are centered in mesopores. Sample LSS1 from Surkhet shows the highest peak at 10 nm diameter with pore volume up to 0.06 mL/g.

Table 2
Elemental mineralogical composition (%) of the shale samples.

Sample ID	Quartz	Pyrite	Siderite	Pl	Ca	Total clay	Clay				BI
							Kaolinite	Chlorite	Illite	I/S	
F298	29.85	0	0	0	0	70.15	10	16	74	0	0.30
F304	22.33	1.87	0	0	27.29	48.51	9	13	78	0	0.23
F280	40.55	0	0	0	0	59.45	11	17	58	14	0.41
F301	38.57	0	0	0	0	61.43	5	8	87	0	0.39
F302	23.32	0	0	10.93	3.21	62.54	7	19	74	0	0.30
F303	30.47	0	0	0	0	69.53	9	13	72	6	0.26
F300	26.83	0	0.89	19.65	2.23	50.40	9	19	72	0	0.33
F306	29.26	0	0	13.76	9.48	47.00	12	18	68	0	0.34

Pl, Plagioclase; I/S, Illite-Smectite ratio; BI, Brittleness Index.

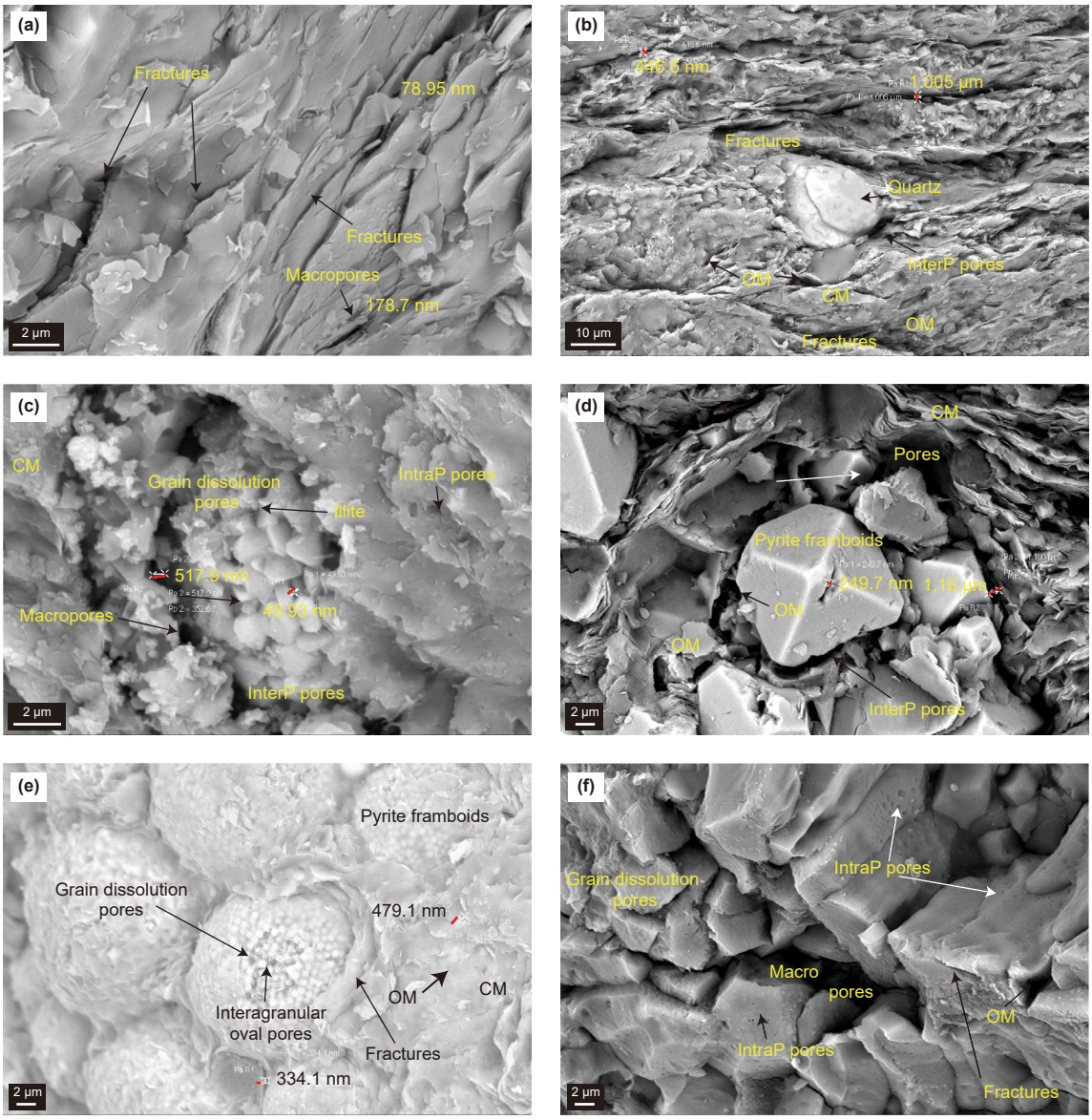

Fig. 5. FE-SEM images showing OM pores observed in the shale samples. Fractures are parallel to each other. (**a**)–(**c**) Shale samples of the Bhainsekati Formation from the Tansen area. (**d**)–(**f**) Bhainsekati shale images from the Surkhet area. Pyrite framboids are observed in samples. Sample F301 is rich in grain dissolution pores, InterP pores are in the nanometer to micrometer range, and fractures are common.

4.4. Low-pressure N_2 and CO_2 gas adsorption isotherms

The nano-scale pore parameters of carbon dioxide adsorption and nitrogen adsorption experimental results are shown in Table 4.

The analysis method combines mercury intrusion and gas adsorption to determine the relative content percentage of micropores, mesopores, and macropores. The BET-specific surface area of the shale obtained from N_2 adsorption ranges from 7.78

Table 3
Summary of MICP analysis data, bulk/grain density, porosity, and permeability values measured on outcrop shale samples from different formations.

Sample	Fm.	Bulk density	Apparent (skeletal) density, g/cm^3	Total porosity, %	Permeability, md	Total intrusion pore volume, g/cm^3	Total pore area, g/cm^3	Median pore diameter (volume), nm	Median pore diameter (area), nm	Average pore diameter (4 V/A), nm
F298	Bk	2.423	2.645	8.413	1.025	0.035	7.243	29.9	9.90	19.20
F280	Bk	2.598	2.682	3.148	9.018	0.012	1.196	1102.2	7.80	40.60
F304	Bk	2.685	2.768	2.999	1.389	0.011	1.148	881.1	6.40	38.90
F301	Bk	2.391	2.610	8.395	0.925	0.035	9.791	13.8	9.80	14.30
F303	Bk	2.486	2.663	6.671	2.468	0.027	5.361	29.1	9.70	20.00
F306	Si	2.632	2.696	2.405	3.016	0.009	0.637	2709.9	5.90	57.40
F300	Si	2.637	2.696	2.181	0.0001	0.008	1.039	1727.6	6.80	31.80

Fm., Formation; Si, Sisne; Bk, Bhainskati.

to 31.21 m^2/g, with an average value of 14.55 m^2/g, whereas the surface area obtained from MICP analysis is 1.038–9.79 m^2/g (Table 5). The maximum amount adsorbed in the Eocene shale, calculated as CO_2 isotherms, ranges from (0.557–12.95) × 10^{-2} cm^3/g, whereas that of the N_2 isotherm BJH pore volume is (9.27–39.9) × 10^{-2} cm^3/g (Table 5). The BJH pore volume of shale varies from 0.01 to 0.418 cm^3/g, with a mean value of 0.019 cm^3/g, and the pore volume obtained from MICP analysis ranges from 0.0082 to 0.0351 cm^3/g. The average pore diameter of the shale sample, calculated by CO_2 adsorption ranges from 1.11 to 1.40 nm, by N_2 adsorption is 35.37–76.90 nm (Table 4), and MICP analysis ranges from 14.3 to 21.72 nm (Table 3). Tables 5 and 6 present these values, with mesopores as the reference point. The multi-point BET model (based on the multilayer adsorption theory) was used in this study to calculate the specific surface area.

The pore size distribution plotted in the relative percentage of pores to specific surface area (Fig. 7(a)) shows that the concentration of mesopores and micropores is higher than macropores. Concerning the relative percentage of pores to pore volume, the concentration of macropores is greater than that of micropores and mesopores (Fig. 7(b)) based on setting the mesopores as the referenced value.

The study employed low-pressure gas adsorption and high-pressure mercury injection methods to examine pores of various shale diameters, yielding pore diameter distributions. Fig. 8 illustrates a wide-ranging distribution of pore sizes and structures from micropores to macropores in the Eocene and Gondwana shale samples determined by all three fluid analysis techniques. Micropores with a pore diameter <1.5 nm was measured by CO_2, and micro to mesopores with a pore diameter ranging from 1.5 to 5 nm were measured by N_2 gas adsorption techniques. MICP techniques measured pore diameters greater than 3 nm. Most of the samples are concentrated in mesopore size, as seen in Fig. 8. To ensure consistency across various methods, CO_2 and N_2 gas adsorption along with MICP data are integrated, aligning units and scales for effective comparison of overlapping pore size areas in shale characterization. Specifically, N_2 mesopores normalize data from N_2 and MICP analyses. This normalization method uses mesopore SA and PV as reference values in Tables 5 and 6 to calculate the relative contents of different pore size distributions.

5. Discussion

5.1. Impact of mineral composition and organic matter on pore structure

The factors influencing pore structure development and evolution of gas shale through diagenesis are its mineral composition and organic matter (Liang et al., 2017; Ross and Marc Bustin, 2009), and play a crucial role in determining gas adsorption capacity (Aringhieri, 2004). The representative Eocene shale samples have higher clay content (>55% on average) followed by quartz, and the illite constitutes over 73% of the clay minerals (Table 2). From the mineralogical and organic carbon analysis, samples with high quartz content have relatively high TOC, especially in samples LHS20 and LSS1. The quartz in the Bhainskati Formation is terrigenous clastic, sourced from Himalayan detritus, with minor authigenic quartz resulting from diagenetic processes (DeCelles et al., 2004). In contrast, biogenic quartz is unlikely due to the absence of siliceous fossils. The study illustrates that clay mineral, mainly illite content, notably impacts the pore structure parameters, precisely SSA, and PV (Fig. 9(a)–(c)). The linear correlation coefficient (R^2) for the Eocene shale samples falls between 0.57 and 0.63 (Fig. 9(a)–(c)), suggesting that pore development within clay minerals consists of micropores and small mesopores. However, a negative correlation is observed between illite content and macropores (Fig. 9(d)), but it is positive for mesopores, indicating that illite mainly influences mesopores. The specific surface area of clay minerals, particularly illite is more significant than that of quartz minerals, which profoundly affects shale reservoirs' physical and chemical characteristics (Milliken et al., 2013). As the clay mineral content increases, the shale's pore structure becomes more intricate, increasing pore volume and surface area, significantly impacting shale gas's adsorption content and capacity (Loucks et al., 2012). In various forms of structural deformation, the SSA falls as the quartz content rises. The clay minerals developed many micropores because of ductile shear deformation.

TOC is a significant factor in shale deformation due to its highly ductile nature, well-cleaved structure, and the overpressures produced by maturation processes (Morley et al., 2017). This study, as well as the previous study, shows that the Eocene Bhainskati shale exhibits 0.7%–5.56% TOC on an average of 1.61% and R_o of 1.83%–2.14% indicating over-maturity (Yang et al., 2021). Porosity, a

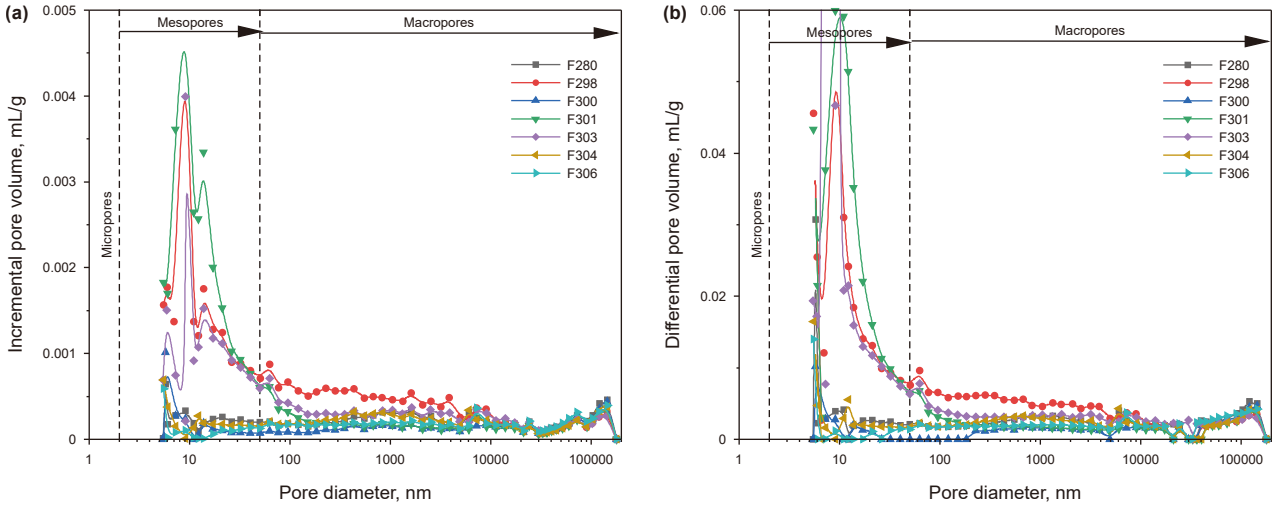

Fig. 6. Pore size distribution of the shale samples. (**a**) Incremental pore volume versus pore diameter and (**b**) differential pore volume versus pore diameter through MICP analysis.

Table 4
Summary of the CO_2 and N_2 Isothermal analysis data of the shale samples.

Sample	CO_2 isotherm analyses			N_2 isotherm analyses		
	Micropore surface area, m^2/g	Micropore volume, $\times 10^{-3}$ mL/g	Average pore diameter, nm	surface area, m^2/g	BJH pore volume, $\times 10^{-2}$ mL/g	Average pore diameter, nm
F280	21.7	7.49	1.38	7.78	9.27	47.67
F300	16.6	5.83	1.40	6.94	13.3	76.90
F301	46.81	12.95	1.11	31.21	39.9	51.09
F302	1.95	0.557	1.14	14.86	19.5	52.54
F304	21.496	7.57	1.41	11.979	10.6	35.37

Table 5
Pore size distribution through pore surface area characteristics of the shale samples.

Sample	Gas adsorption N_2 DFT			MICP			Relative content, %		
	Surface area, m^2/g	Micropore	Mesopore	Mesopore	Macropore	Surface area, m^2/g	Micropore, %	Mesopore, %	Macropore, %
F298	8.560	5.960	2.600	7.240	0.184	7.424	51.2	47.0	1.8
F280	7.780	5.075	2.705	1.139	0.057	1.196	48.3	48.2	3.5
F304	11.979	8.600	3.379	1.088	0.060	1.148	51.8	44.4	3.8
F300	6.940	3.134	3.806	1.009	0.029	1.038	36.4	61.3	2.3
F301	31.212	19.814	11.398	9.698	0.092	9.790	48.0	51.3	0.7
F303	22.350	12.430	9.920	5.348	0.012	5.360	435	56.3	0.2
F302	14.860	1.950	12.910	6.516	0.035	6.550	12.3	87.2	0.5

* The relative contents of different pore size distributions with SA were calculated by setting the mesopore SA (DFT) as the referenced value.

Table 6
Pore size distribution from pore volume characteristics of the samples.

Sample	Gas adsorption N_2 DFT			MICP			Relative content, %		
	Pore volume, mL/g	Micropore	Mesopore	Mesopore	Macropore	Pore volume, mL/g	Micropore, %	Mesopore, %	Macropore, %
F298	0.012	0.004	0.009	0.020	0.015	0.035	21.5	47.4	31.1
F280	0.010	0.002	0.008	0.003	0.009	0.012	16.2	34.5	49.3
F304	0.013	0.004	0.009	0.003	0.008	0.011	20.7	30.2	49.0
F300	0.011	0.002	0.009	0.002	0.006	0.008	09.9	39.5	50.5
F301	0.042	0.009	0.032	0.028	0.007	0.035	18.6	64.1	17.3
F303	0.035	0.008	0.027	0.016	0.011	0.027	17.4	52.0	30.6
F302	0.021	0.004	0.016	0.017	0.006	0.023	17.5	62.4	20.1

* The relative contents of different pore size distributions with PV were calculated by setting the mesopore PV as the referenced value.

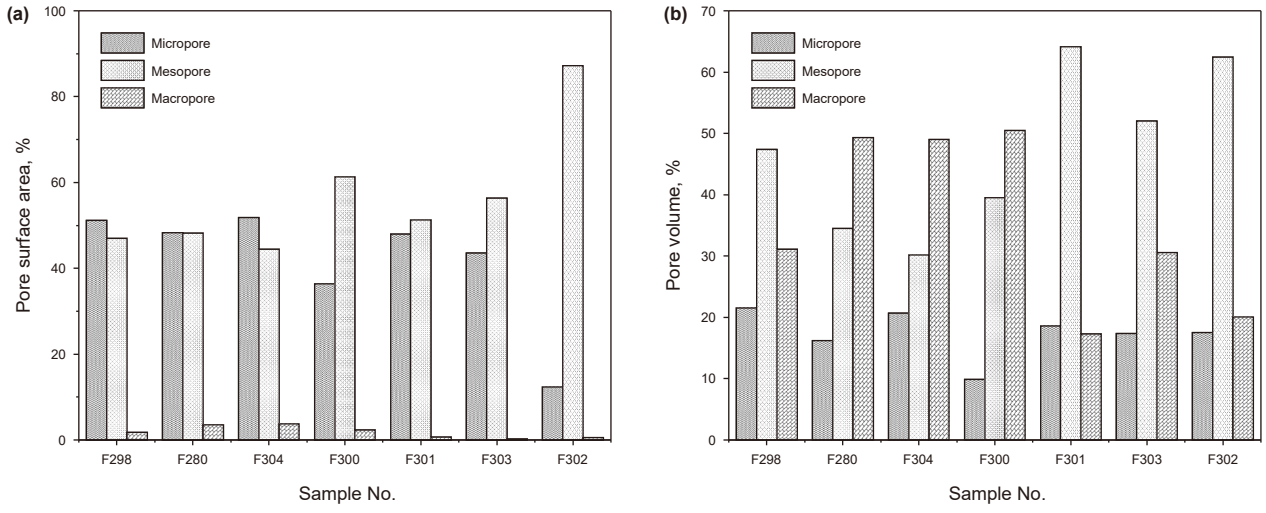

Fig. 7. The pore size distribution based on (**a**) pore surface area and (**b**) pore volume for shale samples.

critical property of shale gas reservoirs, measures the void space within organic-rich rocks, governing gas storage capacity and fluid flow dynamics. The plot of porosity with clay, quartz, and TOC exhibits a positive correlation (Fig. 10), suggesting that the overall porosity of shale is dependent on mineral content (Chalmers et al., 2012) and TOC, while the correlation is negative with the thermal maturity (Fig. 10(c)). The Bhainskati shale is clay-rich, which could reduce porosity despite increasing maturity (Khadka et al., 2024).

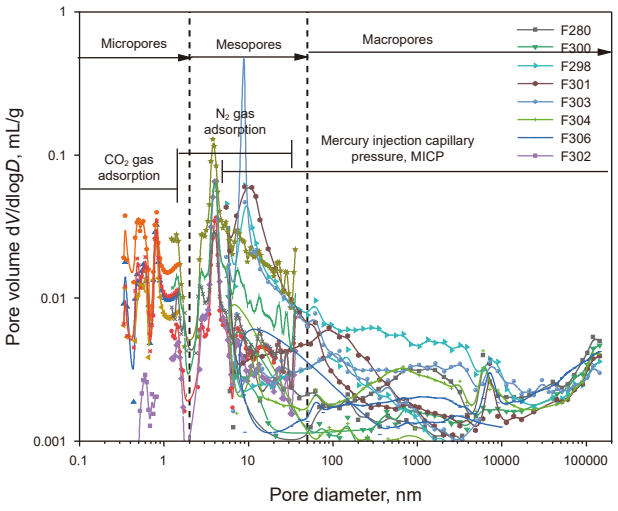

Fig. 8. Pore volume distribution curves from low-pressure gas (N_2 and CO_2) adsorption and MICP in different shale samples.

Porosity increases with increasing quartz content (Fig. 10(b)). The plotted data might represent samples where TOC is insufficient to drive significant porosity development. The Bhainskati shale's inverse porosity-maturity trend likely results from compaction/cementation dominating over OM porosity creation, possibly due to low initial TOC and clay diagenesis (Khadka et al., 2025).

SEM observations corroborate this finding. High mineral content and numerous interparticle pores between quartz grains and clay particles may contribute to the porosity in these Eocene Bhainskati shale samples (Fig. 5). A series of tectonic movements has widely deformed the Eocene Bhainskati shale strata. The interplay between mineralogy, TOC content, and thermal maturity significantly influences shale pore structure and gas sorption characteristics. Shale pore structure and gas storage are influenced considerably by shale composition, with hydrocarbon generation from organic matter driving pore development. This process is minimal below a thermal evolution threshold (R_o < 0.90%) and increases substantially until R_o exceeds 6.36% in the Woodford shale samples (Curtis et al., 2012; Ju et al., 2018). Fig. 11(a) shows a positive correlation between TOC and porosity in the Shale of the research area, which indicates that organic carbon is a key pore

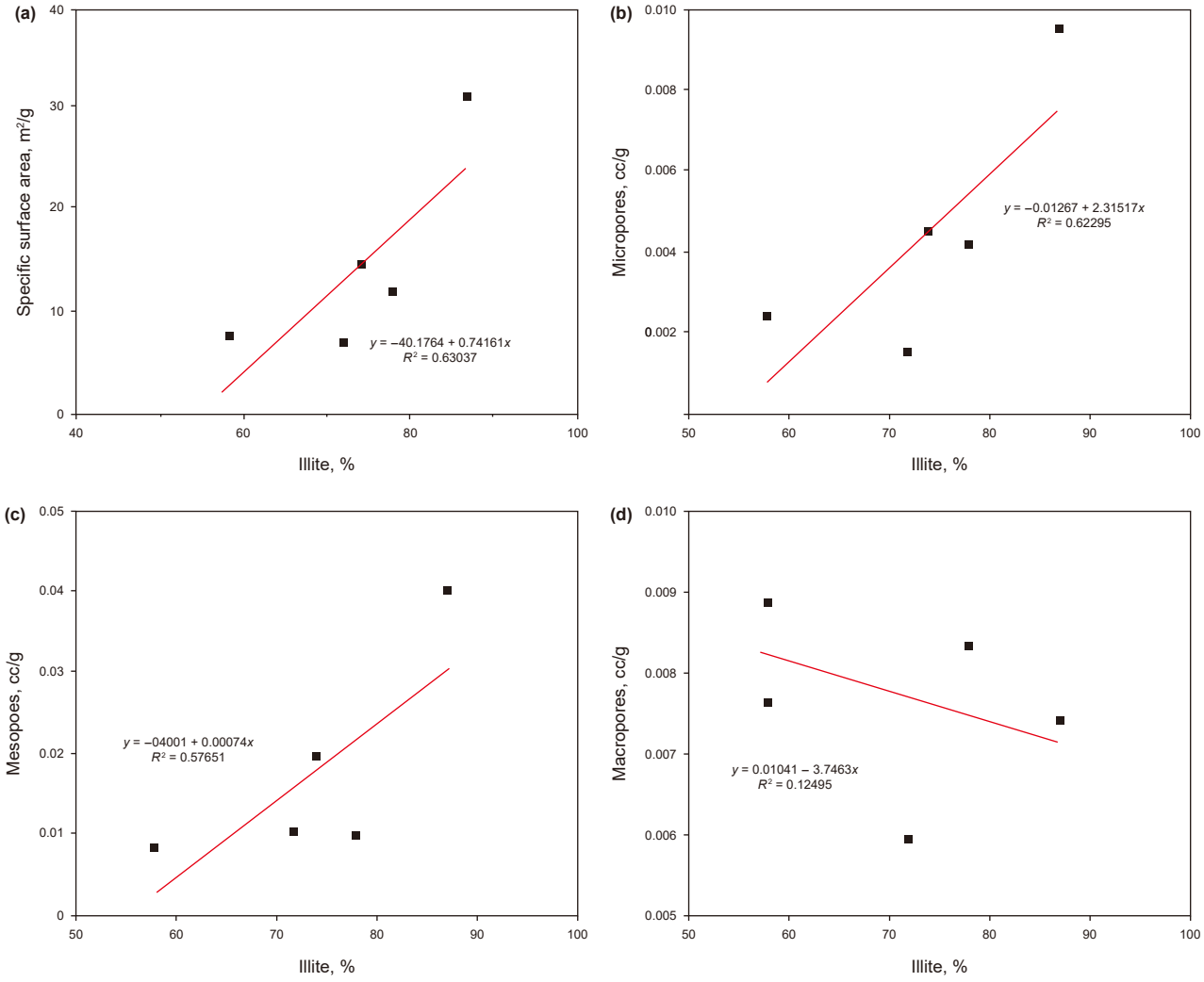

Fig. 9. The correlation between Illite content and various pores of shale samples. (**a**) Illite versus specific surface area. (**b**) Illite versus micropores. (**c**) Illite versus mesopores. (**d**) Illite versus macropores.

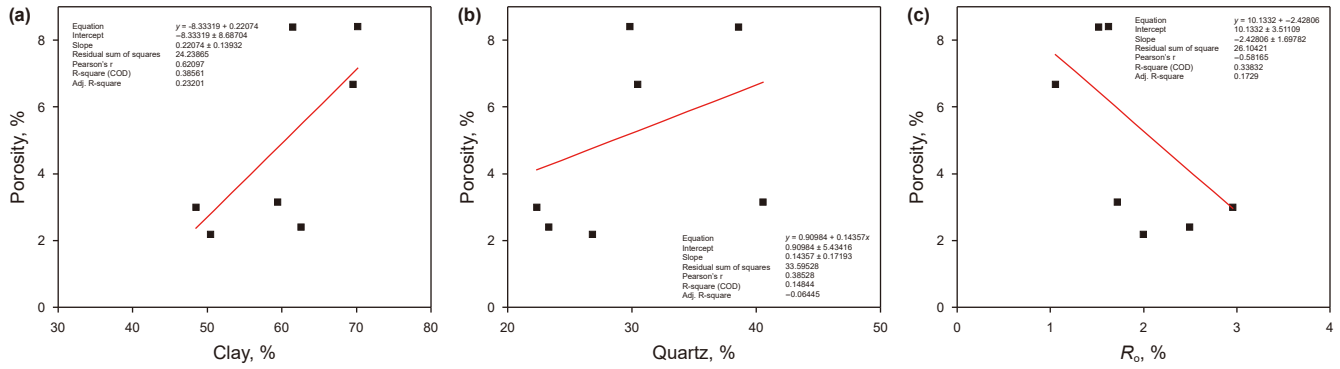

Fig. 10. Correlation of porosity with mineral content and thermal maturity. (**a**) Porosity versus clay content. (**b**) Porosity versus quartz content. (**c**) Porosity versus Vitrinite Reflectance (%R_o).

controlling factor. However, with the moderate correlation ($R^2 = 0.47$), shale pore development is also influenced by other factors. Thermal maturation processes are influenced by tectonic movements such as the Himalayan orogeny, further shaping the shale pore structure. Compaction during early diagenesis densifies pores, while later pyrolysis generates hydrocarbons, developing organic pores (Loucks et al., 2012). Tectonic activity in the Himalayan region induces fractures in shale, significantly enhancing permeability despite porosity reduction from compaction. This alteration redistributes and aligns pores and fractures to create efficient flow pathways, emphasizing connectivity and distribution of microfractures and organic pores in the complex Eocene foreland shale. The Bhainskati shales are dense with low permeability, ranging from 0.925mD to 9.01mD (Table 3). Tectonic stress generates microfractures and reactivates existing fractures, creating high-conductivity pathways (Ju et al., 2018). This results in higher permeability despite lower porosity (Fig. 11(b)). Himalayan tectonics produces preferential fracture alignment along shear zones (Dhital, 2015).

The total organic carbon and gas content have a direct relationship with tectonic disruption, and the gas content has a positive relationship with the TOC as free gas or absorbed gas in or on the organic matter pores (Loucks et al., 2009; Milliken et al., 2013). The complex relationships between compaction, tectonic activity, and varied preservation and destruction of pore structures are the primary contributing factors to the fragile relationship between TOC and porosity in the Eocene foreland shale samples (Fig. 11(a)). As shown in Fig. 11(a), the expected positive correlation is overprinted by the competing effects of tectonic deformation, explaining non-linear relationship observed in our analyzed samples. Under tectonic stress, OM pores are especially prone to collapsing. InterP pores can be compressed and reshaped by tectonic forces, breaking the correlation between TOC and porosity (Xiao et al., 2021). In addition, the pore network of the shale is diverse, and differences in thermal age affect how OM pores form and collapse. Even in samples with high TOC, porosity decreases as newly created pores contract as thermal maturity increases.

Furthermore, the multiscale and stages of tectonic movements in the study area have formed thrusts, faults, and klippes, significantly impacting shale gas preservation conditions within the same rock strata. Many previous studies have proved that the TOC has influenced the total pore volume and the micropores and mesopores (Chalmers and Bustin, 2007; Zhang et al., 2020). A positive correlation exists between shale gas content and adsorption capacity with TOC concentration (Ross and Marc Bustin, 2009; Xiong et al., 2017; Zhang et al., 2012). Fig. 12 shows the impact of TOC content on shale pore structure parameters. In this study, the TOC content of the representative samples shows a positive relation with pore volume and surface area but a hostile relation with average pore diameter (Fig. 12), implying that the organic matter micropores are easily affected. The linear correlation coefficient of the TOC content and specific surface area is

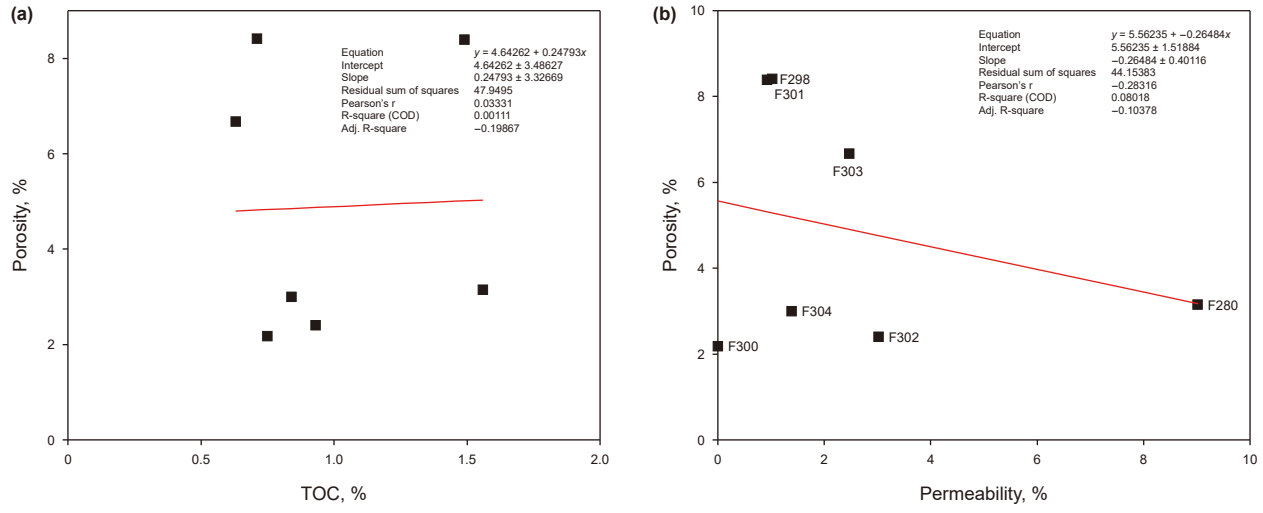

Fig. 11. Correlation of porosity of shale with TOC and permeability. (**a**) Porosity versus TOC. (**b**) Porosity versus permeability.

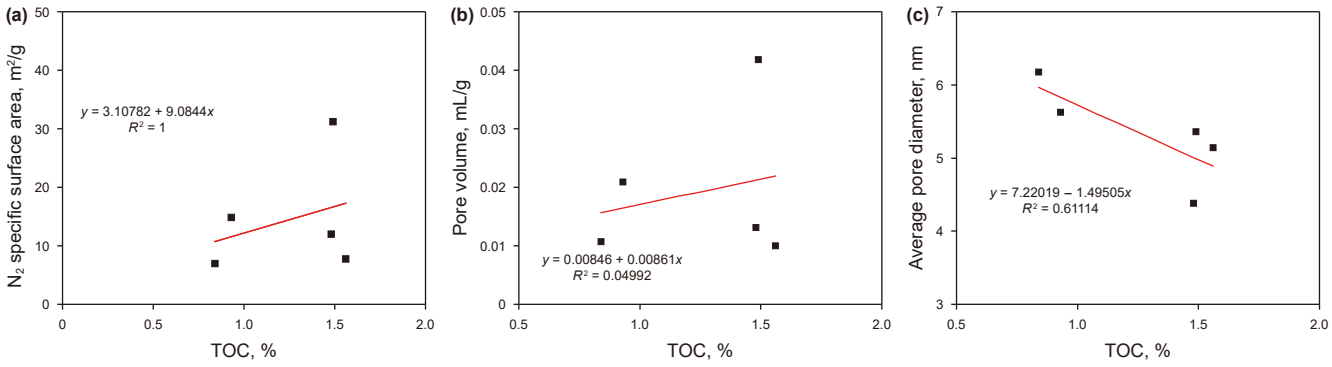

Fig. 12. TOC correlations with pore structure characteristics. (**a**) TOC versus specific surface area. (**b**) TOC versus total pore volume. (**c**) TOC versus average pore diameter.

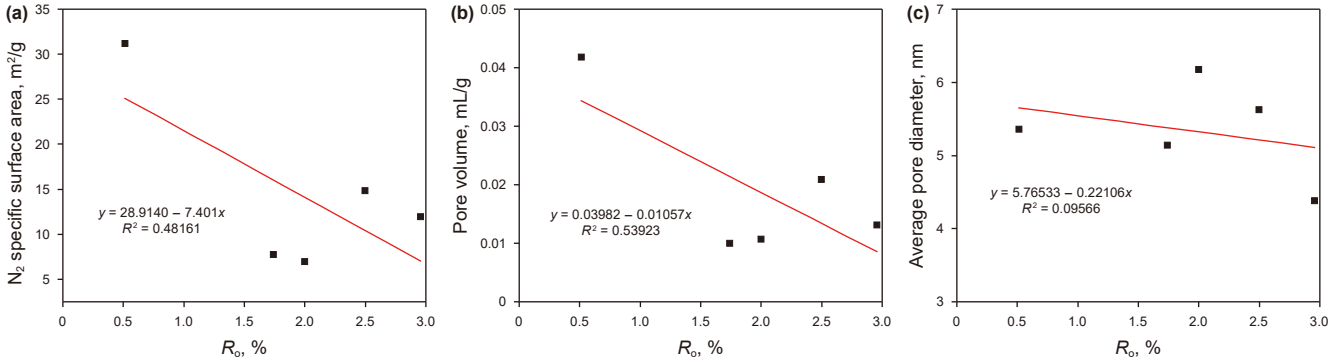

Fig. 13. Relationship between thermal maturity (R_o) and pore structure characteristics. (**a**) R_o versus specific surface area. (**b**) R_o versus total pore volume. (**c**) R_o versus average pore diameter.

greater than that of the pore volume (Fig. 12(a)–(b)), indicating that the effect of the TOC content on the surface area is more significant than that of the pore volume.

The micropores of organic materials were the primary source of the large specific surface areas in the shales with higher TOC contents. The relationship between specific surface area, pore volume, and pore size and thermal maturity (R_o) in different gas-content shales is illustrated in Fig. 13, where no perfect relationship was observed in the analyzed samples. With increased maturity often enhancing organic porosity and surface area in many shale systems, our data from the tectonically active Himalayan setting reveal a different trend. As illustrated in Fig. 13(a) and (b), both specific surface area and pore volume exhibit a clear negative correlation with vitrinite reflectance (%R_o), indicating that these properties decrease as thermal maturity increases. This deviation from the conventional trend may be attributed to the unique geologic history of the Eocene Bhainskati shale, where intense tectonic compression and associated thermal stress have

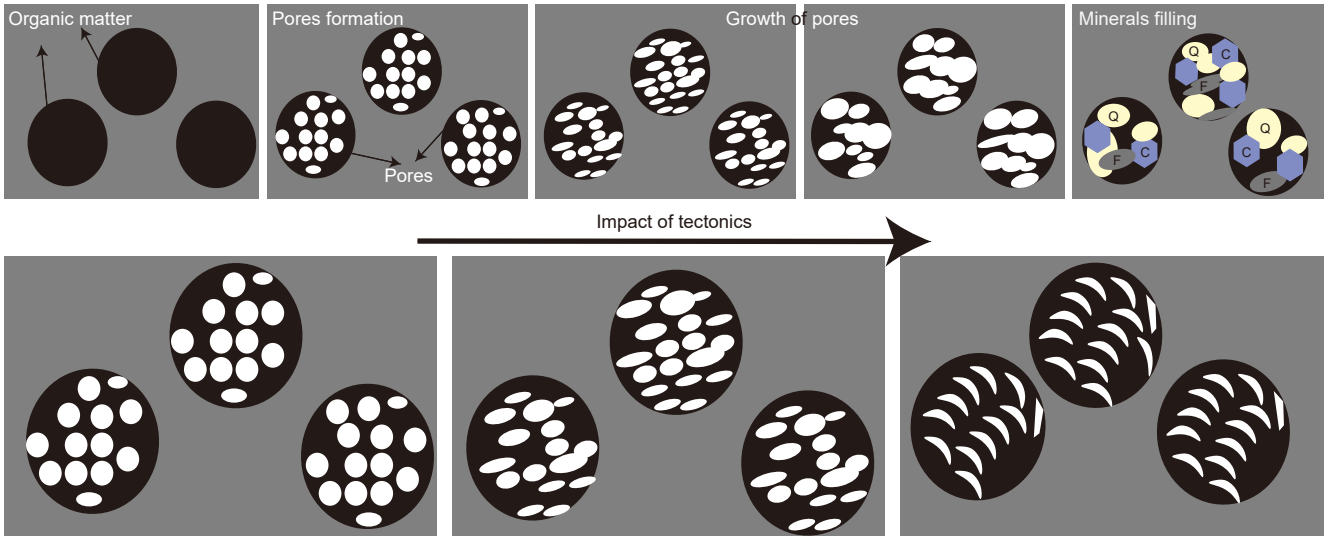

Fig. 14. Organic pore evolution schematic model showing (**a**) organic pores related to hydrocarbon maturation and (**b**) the impact of tectonic deformation on organic pores.

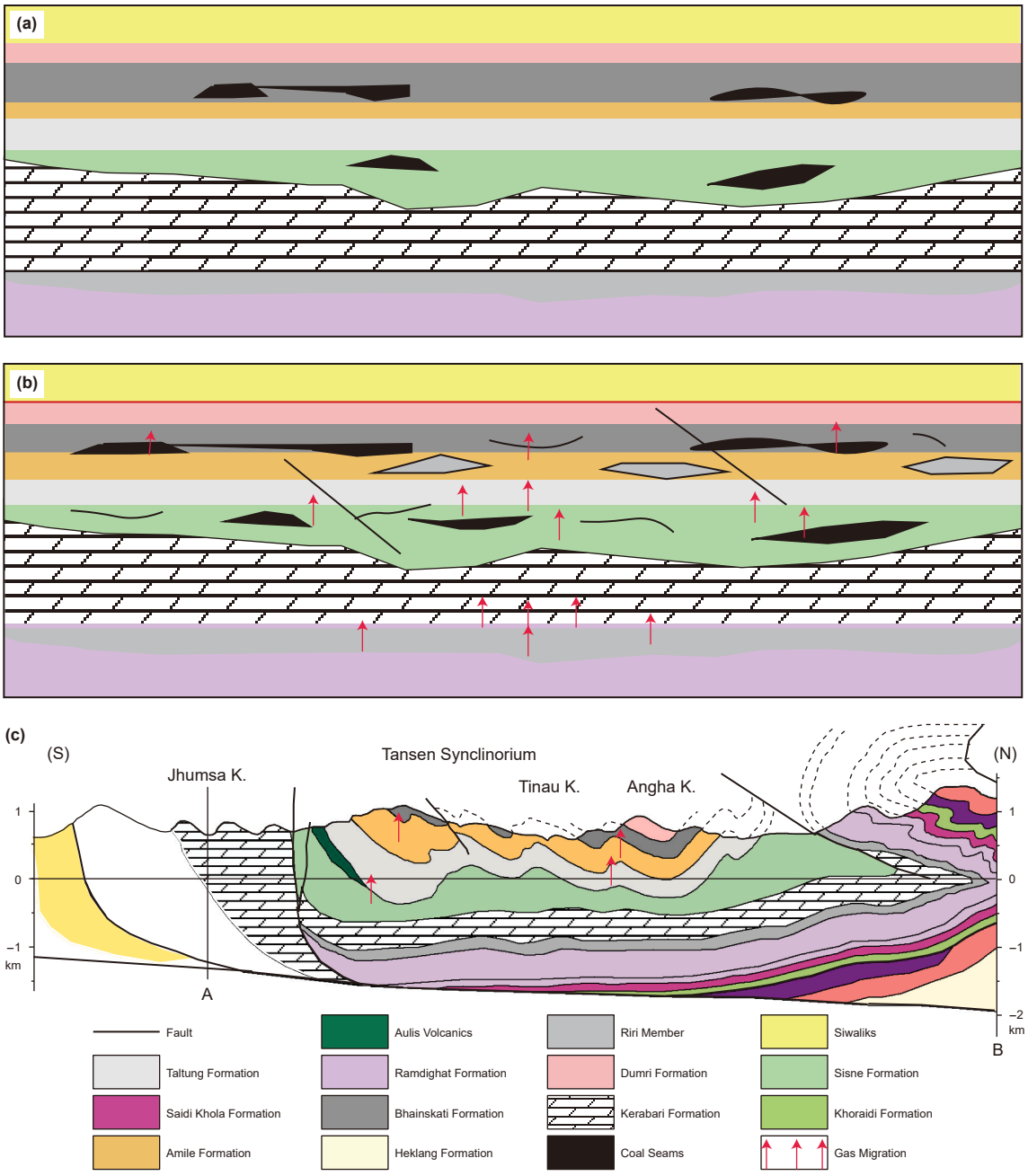

Fig. 15. Schematic model of natural gas accumulation, preservation, and migration in the Tansen Area, Nepal. (**a**) Gas accumulation model. (**b**) Preservation and migration of the gas. (**c**) Present geological profile of the Tansen area (modified after Sakai, 1983).

likely promoted excessive organic matter condensation and pore collapse during overmaturation, reducing surface area and mesopore volume despite advanced maturity. In contrast, the increase in thermal maturity has a slow decline in average pore diameter (Fig. 13(c)). This relation exhibits the positive impacts of the Himalayan tectonism on the thermal maturity of the Eocene shale, leading to dry gas generation and causing a decrease in specific surface area, pore volume, and pore diameter.

The pore structure and gas sorption characteristics of the Eocene foreland Bhainskati shales are influenced by a combination of factors, including mineralogy, TOC, and thermal maturity. For this reason, the shale's TOC content is also insufficient (<2%). The tectonic impact has influenced the gas adsorption capacity of the shale. The limitation of the outcrop sample analysis in the current study suggests further research and exploration with drilling, which can enhance our understanding of shale pore characteristics and reservoir behavior in the tectonically deformed area of the Himalayas Eocene shale.

5.2. The shale reservoir formation and effects of tectonic deformation on pore structure

The Bhainskati Formation shale reservoir originated in a syn-collisional foreland basin during the Eocene, where marine to shallow-marine deposition under restricted circulation preserved organic matter sourced from terrestrial detritus and marine plankton (Sakai, 1983). In many foreland basin shales, inorganic pores (e.g., clay-related, intergranular) often dominate over OM

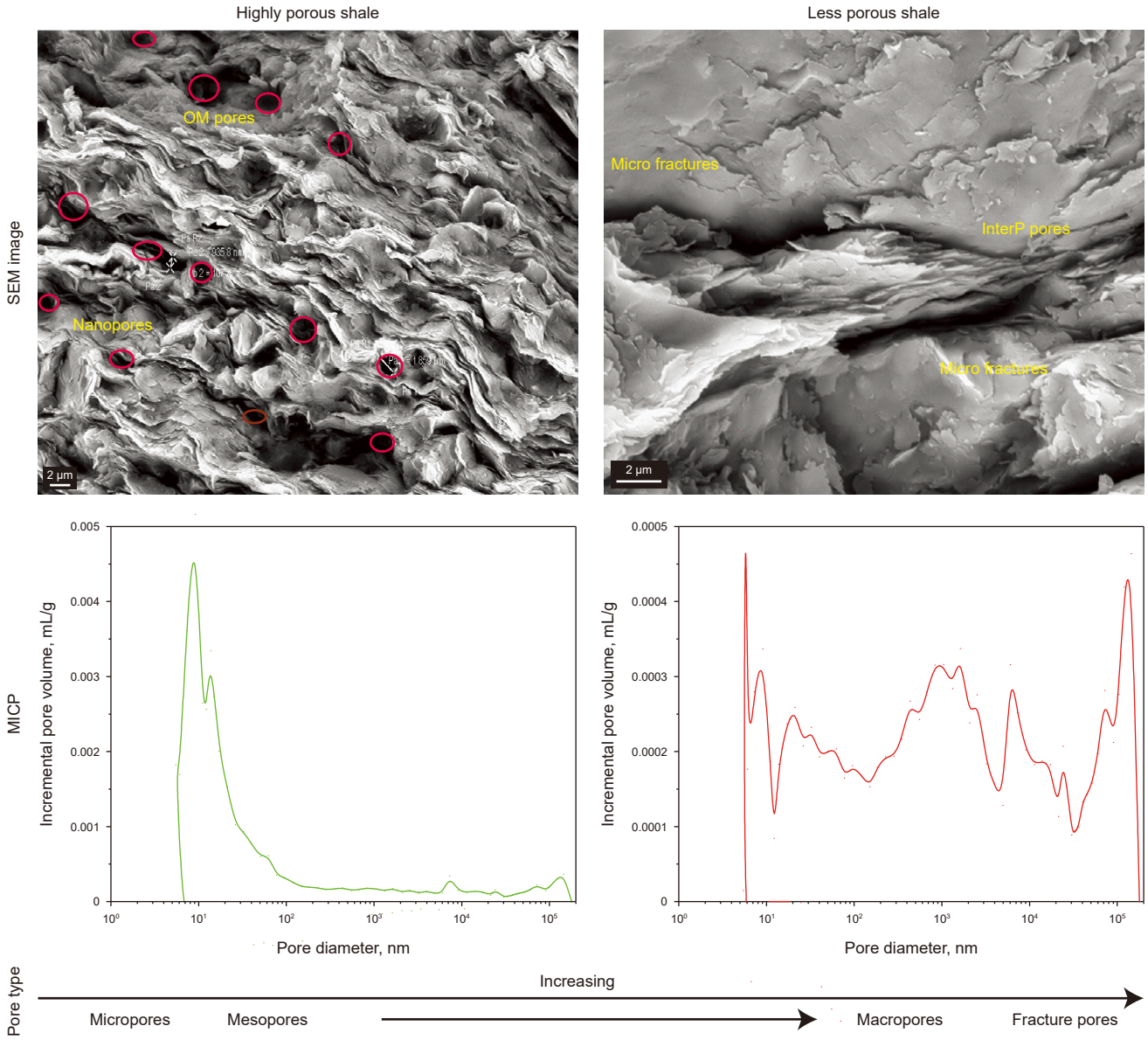

Fig. 16. Comparative pore characteristics through MICP and SEM analysis of different gas-bearing shale samples. (**a**) High gas-bearing sample LSS1, Surkhet area. (**b**) Low gas-bearing sample LHS20, Tansen area.

pores due to high clastic input and diagenetic overprinting (Decelles, 2012; DeCelles et al., 2004). As the India-Eurasia collision progressed, rapid subsidence and burial (3–5 km depth) subjected these OM-rich silty shales to temperatures within the gas window (120–200 °C), driving thermal maturation of Type II/III kerogen (Wang et al., 2023). The organic carbon content in shale affects the development of pores in shale through hydrocarbon generation. Hydrocarbon generation via kerogen cracking produced organic-hosted nanopores (20–200 nm), predominantly bubble-shaped and isolated within OM (Fig. 14(a)). These pores, critical for adsorbed gas storage, formed as volatiles escaped during OM transformation, creating a network of nano-to micro-scale voids. Early diagenetic processes, including smectite-to-illite conversion and quartz cementation, reduced primary porosity but enhanced brittleness, while maturation-induced microfractures improved pore connectivity. High mechanical stress in foreland basins preferentially collapses OM pores, leaving fractures as the primary voids. The resulting pore structure, comprising OM pores, interparticle voids, and microfractures, dictated the shale's dual capacity for gas storage, adsorbed in micropores, and the migration of free gas in fractures. While hydrocarbon generation created isolated OM-hosted nanopores (Fig. 14(a)), their limited connectivity suggests that gas storage and flow rely more on fractures and interparticle pores (Fig. 14(b)), which is also observed in the SEM images shown in Fig. 5. The primary role of OM may be gas adsorption rather than porosity development.

The development of organic pores is controlled by the thermal evolution degree (Curtis et al., 2012). Organic pores in shale, often bubble-shaped and isolated within organic matter (Fig. 14(a)), facilitate the creation of interconnected pore networks (Zhu et al., 2018). These pores are vulnerable to external factors like fluid injection, cementation, and tectonic stress due to the soft nature of the surrounding organic matter. As hydrocarbon maturation progresses, organic pores evolve through development, growth, and mineral infilling (Fig. 14(a)). The structure of organic pores changes with the increase of burial depth during pyrolysis and hydrocarbon

generation of organic matter. As the shales undergo compaction and tectonic deformation, the pores become less rounded, exhibiting more branch-like and line-like edges in directional alignment due to the absence of mineral support and protection (Fig. 14(b)). Post-depositional Himalayan tectonics dynamically reshaped OM pore networks. Syn-orogenic thrust loading (MCT) accelerated burial and thermal stress, optimizing OM pore development during peak gas generation. However, subsequent tectonic compression and shear induced ductile deformation, dispersing OM within clay matrices and elongating pores into branch-like structures (Fig. 14(b)), reducing roundness and increasing specific surface area for enhanced adsorption. Tectonic deformation is one of the important reasons for the occurrence of reservoir pore deformation (Li et al., 2021). The regional thrust and faults increase the pressure and temperature, eventually providing sufficient thermal maturity for gas generation of the Bhainskati shale in the Paleocene (Wang et al., 2023). The gas starts to migrate and accumulate in the source rocks, with the fracture developed by local faults helping to migrate to the upper sandstone layers for preservation (Fig. 15(a)–(b)). In the Eocene shale in the Lesser Himalayas, Nepal, the organic matter pores and microfractures were crucial for gas retention, as these features provided storage space and pathways for gas migration (Fig. 15(c)).

Gas-bearing shale features numerous organic pores, ranging from nanometers to micrometers, with minimal micro-fractures. Based on pore diameter (D), macropores ($D > 50$ nm), mesopores ($D = 2$–50 nm), and micropores ($D < 2$ nm) can be identified (IUPAC, 1994). Mesopores have the most significant average pore volume, followed by macropores and micropores. However, as shale shifts from brittle to ductile deformation, there's a gradual increase in the contribution of mesopores and micropores while macropores diminish (Ju et al., 2018). Similarly, mesopores dominate the average specific surface area, followed by micropores, with macropores showing a negligible contribution that wanes with increased deformation. Mesopores and micropores collectively contribute the most to the average specific surface area, and concerning pore volume, macropores and mesopores are higher than that of the micropores (Fig. 7). From the analysis, it is observed that the mesopores contribute the highest pores both in pore surface area and pore volume. However, in the case of the samples close to the tectonic zone, the macropores contribute more to pore volume. This variation in pore size could be a reason for a tremendous change in the morphology and structure of the area due to the immense tectonic activity that produces local and regional structures. These representative samples in the study area clearly show that pore volume is more affected by tectonism than surface area, contributing to a higher percentage of macropores. Micropores and mesopores primarily facilitate gas adsorption and storage, while organic and intergranular pores are predominant in gas adsorption and microfracture for free gas storage (Xu et al., 2020). Consequently, shale reservoirs evolve into complex dual-porosity systems comprising various pore types, including micro-, meso-, and macropores, and microfractures, which are crucial for gas transport and storage (Feng et al., 2022). The proportion of meso- and macropores increases with deformation, accompanied by enhanced permeability, while micropores gradually decrease. In the sample analyzed, we observed that most of them are concentrated in mesopores, with a pore diameter of 5–10 nm (Fig. 8). Furthermore, shale reservoirs exhibit regional variability in pore characteristics influenced by geological tectonics. This pore network is more connected and open (W. Sun et al., 2020). During the pyrolysis and hydrocarbon generation of organic matter, the structure of organic pores changes with the increase in thermal maturity, with micro and meso pores shrinking under extrusion and becoming directionally aligned as indicated by the red circle in Fig. 16(a). The distinct spongy, bubble-like morphology of the features observed in Fig. 16(a) is characteristic of secondary organic porosity formed during hydrocarbon generation. This is inconsistent with the sharp, angular, or cleaved surfaces typical of brittle mineral detachment.

Gas movement in highly porous shale primarily occurs through sorption and diffusion, with microfractures acting as conduits for free gas migration via Darcy flow and serving as storage sites if sealed by mineralization. In contrast, low gas-bearing shale relies on Darcy flow, mainly containing free gas. Pore throat size controls both the flow mechanism and, indirectly, the gas storage capacity. The MICP study indicates that high gas-bearing samples exhibit a tiny pore throat diameter compared to low gas-bearing samples

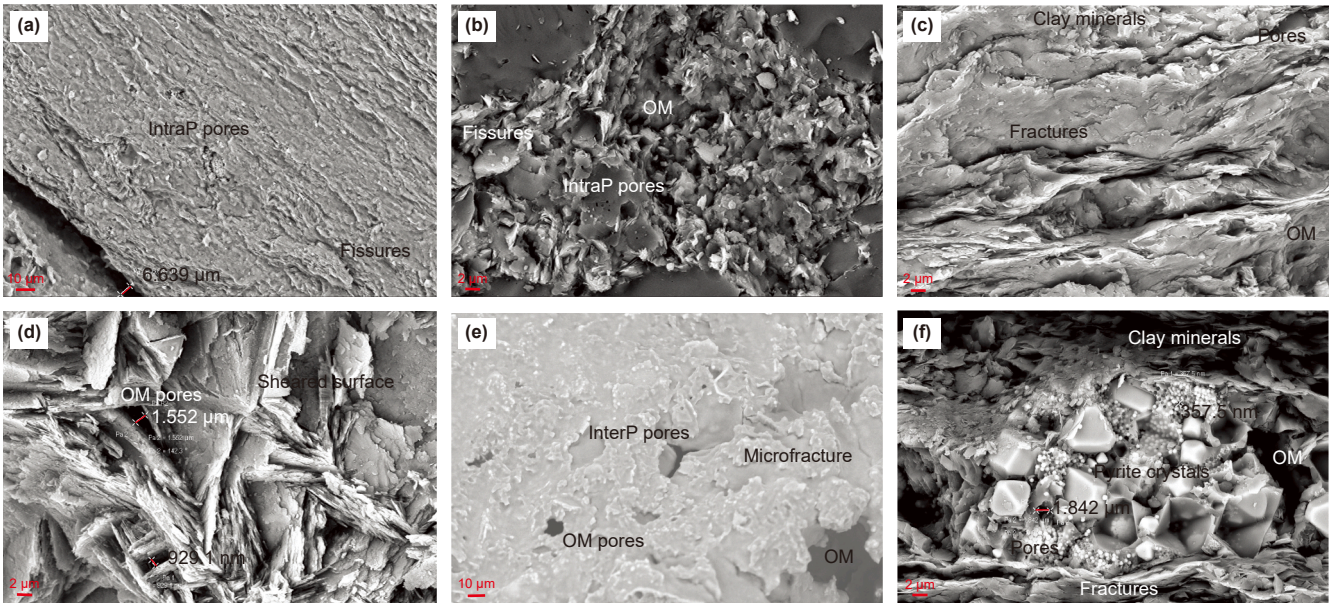

Fig. 17. SEM images showing fractures and microstructural fractures in strongly deformed shales from the Tansen area (**a**)–(**c**) and the Surkhet area (**d**)–(**f**).

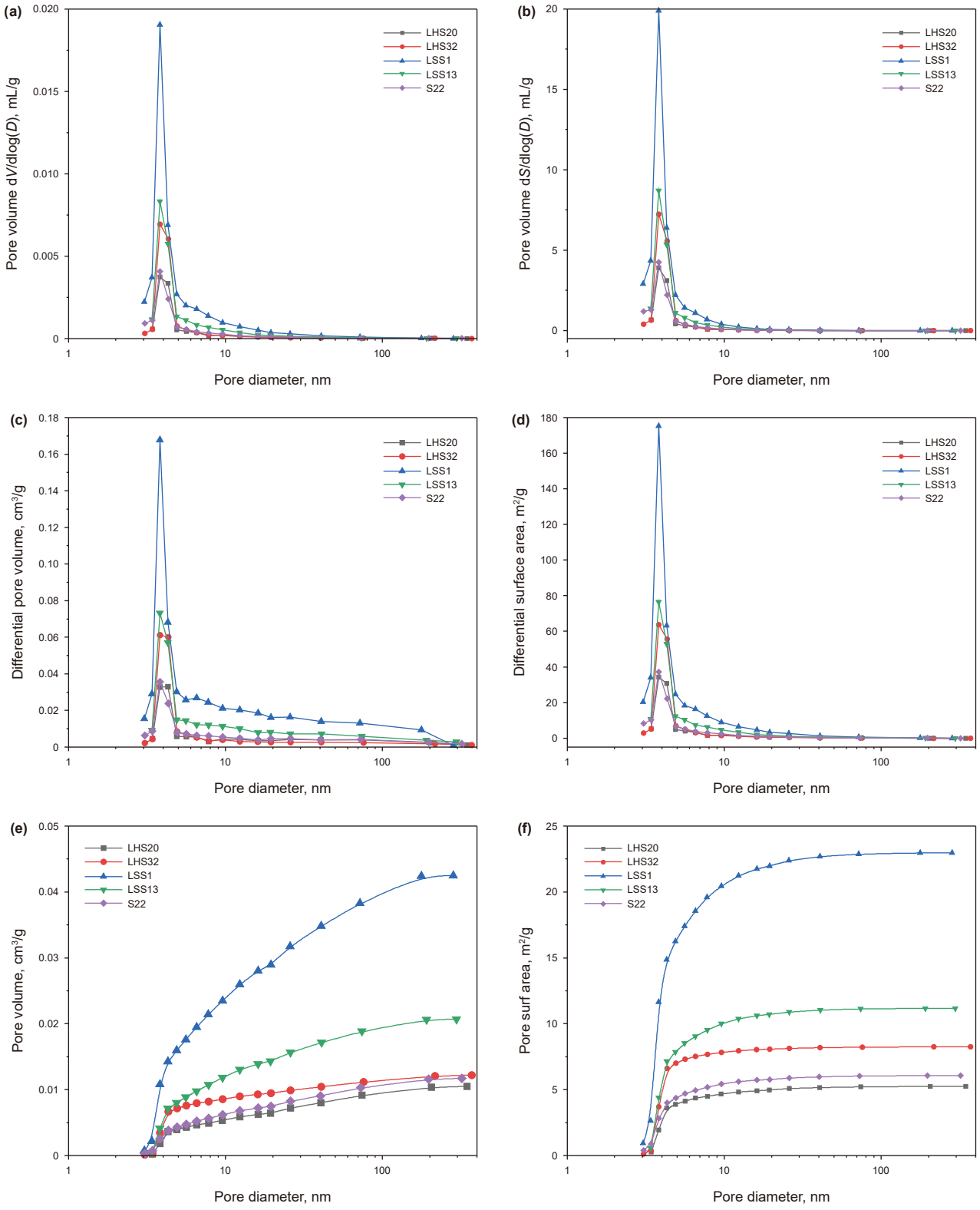

Fig. 18. BJH pore size distributions from N_2 desorption Isotherms of shale samples. (**a**) Pore diameter versus differential pore volume (d*V*/dlog(*D*)). (**b**) Pore diameter versus differential surface area (d*S*/dlog(*D*)). (**c**) Pore diameter versus differential pore volume. (**d**) Pore diameter versus differential surface area. (**e**) Pore diameter versus cumulative pore volume. (**f**) Pore diameter versus cumulative surface area.

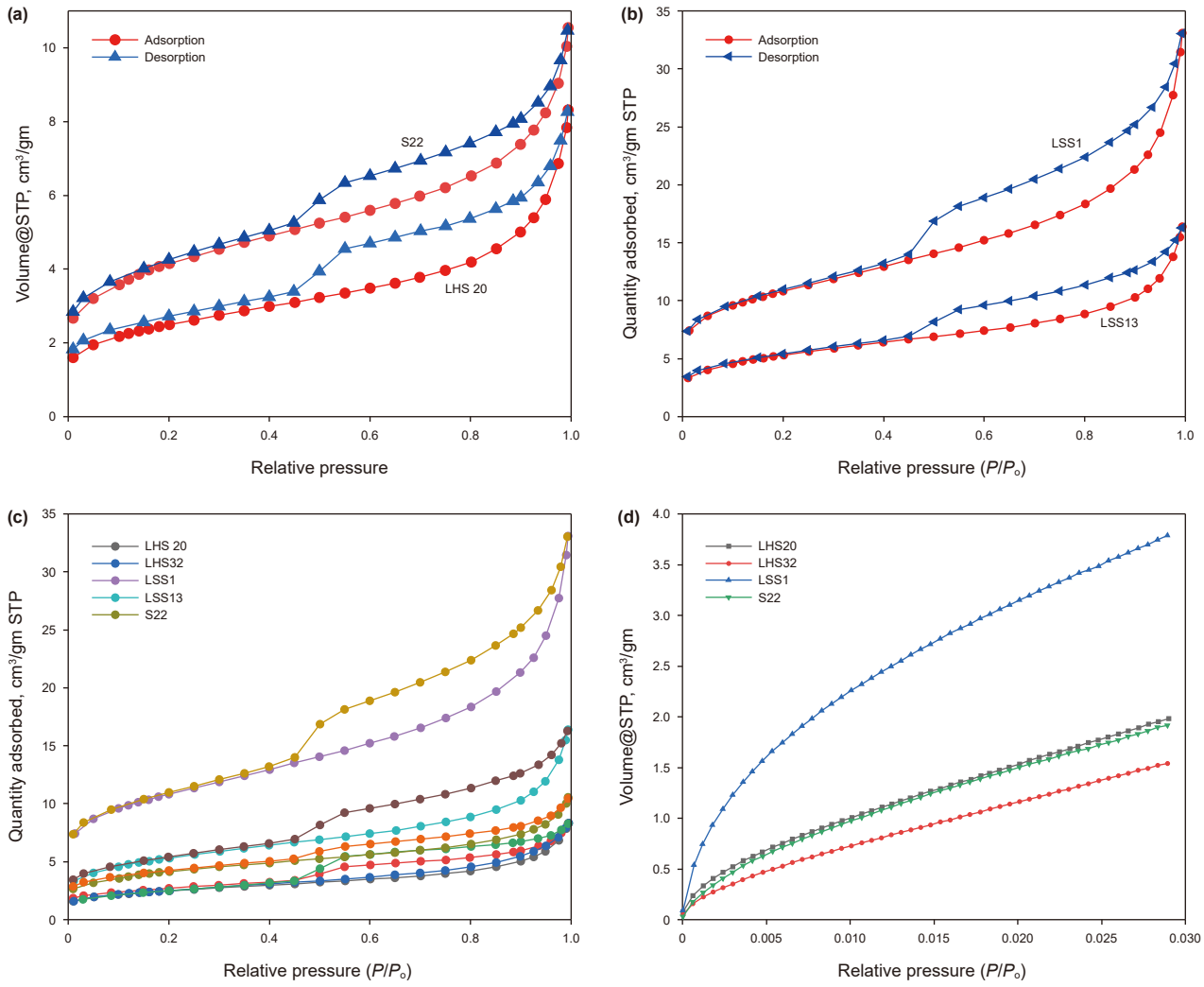

Fig. 19. Low-pressure gas adsorption-desorption isotherms curve of shale samples. (**a**) N_2 isotherms of the Tansen area samples. (**b**) N_2 isotherms of the Surkhet area samples. (**c**) N_2 isotherms of all samples together. (**d**) CO_2 isotherms of all samples together.

(Fig. 13). Shale with better pore connectivity facilitates gas transport, enhancing reservoir permeability. Internal micro-fractures, detected through FE-SEM imaging, serve as dominant pathways for gas transport despite their small volume contribution (Fig. 5). The fracture aperture of the Bhainsekati shale is found to be almost one μm (Fig. 16). Microfractures, alongside the pore system, play a pivotal role in governing gas storage and transport processes, influencing the Eocene shale permeability anisotropy under varying stress conditions. FE-SEM imaging confirms the presence of microfractures with apertures of ~1 μm (Figs. 5 and 16); their effectiveness under subsurface stress conditions is a function of their mineralogy and connectivity. The high quartz content and early cementation observed in the Bhainskati shale (Table 2, Fig. 4) suggest that many fractures may be 'propped' open by brittle minerals, enhancing their sustainability. Furthermore, the alignment of fractures relative to the present-day in-situ stress field will ultimately determine their contribution to permeability anisotropy. Organic porosity is contingent on thermal maturity and organic matter composition, significantly impacted by tectonism (Loucks et al., 2012). Overmaturity can weaken organic porosity and damage the microstructures of OM pores. The pores between organic grains and clay flakes are significantly impacted by tectonic deformation, but other rigid mineral pores don't suffer such a drastic loss of shape (Zhu et al., 2018).

The pore structure of shale samples seems less affected by deformation if the samples are away from significant tectonic structures like MCT, MBT, and other locally developed structures such as fault, thrusts, joints, and other linear features. However, both organic and inorganic pores in fold-related and near-fault shale samples have the characteristics of increasing pore size, better connectivity, and growing microfractures, as observed in SEM images (Fig. 17). The presence of pyrite crystals (Fig. 17(f)) and the development of nanoparticles and organic layers are regarded as signs of the occurrence or enhancement of faults or shear.

SEM images reveal a diverse range of interparticle pores, spanning from 200 nm to 2 μm, with an irregular spatial distribution. These pores may originate from various processes such as bioturbation, hydrocarbon generation, and tectonism (Loucks et al., 2012). In the Eocene Bhainskati shales, remnants of bioturbation are evident, alongside significant regional and local tectonic effects. Interparticle pores typically form at the triple junction of mineral grains, exhibiting higher connectivity and interconnection compared to intraparticle pores (Fig. 17(e)). Intraparticle pores, mainly found in carbonate particles due to late diagenetic dissolution, possess moderate connectivity but are less abundant and smaller in size. Tectonic deformation strongly influences pores within or between organic grains and clay flakes, contrasting with rigid mineral pores that maintain their shape

more effectively. These open microstructures, often exceeding 0.1 μm in width and 10 μm in length (Fig. 17(a)), serve as migration pathways for hydrocarbon molecules. Notably, heart-shaped pyrite accumulations in the shale sample contain numerous microchannels and fractures within their oriented and fractured structure, significantly impacting shale porosity and permeability (Figs. 17(f) and 5(c)). The SEM images (Figs. 5 and 17) depict various pore types and micro-channels, possibly attributed to tectonic activity. Interconnected microfractures of varying sizes serve as vital transport channels for shale gas, facilitating its enrichment and migration. The connectivity of interparticle pores via microchannels and fractures establishes pathways for gas storage and migration, highlighting the significant impact of tectonism on deformed Himalayan shale. Furthermore, this tectonism affects the different strata within the same formation and the pore structure and accumulation pattern within the same rock strata.

Notably, a significant amount of gas is adsorbed in small micro-mesopores, indicated by the continuous rise in [dV/d(d)] from macropores to mesopores (Fig. 18). Pore sizes between 3 nm and 10 nm exhibit the highest pore frequency accompanied by a decrease in pore size and an increase in pore volume, suggesting a significant influence of pore size and geometry on adsorption capacity. The pore size distribution in the Tansen and Surkhet regions is similar (Fig. 18), but the pore area and volume in the Surkhet area are higher than in the Tansen area. Micropores and mesopores mainly occupy the pore volume. Additionally, a larger pore volume corresponds to a smaller pore size and a higher storage capacity, as evident from Tables 5 and 6 Notably, the PSDs of shale samples reveal single prominent peaks in the curves of dV/dlog(D), dS/d(D), and dS/dlog(D) (Fig. 18(a)) around the artificial 4 nm peak. Furthermore, the curves exhibit unimodal pore peaks within the range of 1–10 nm (Fig. 18(b)–(d)), indicating that micropores and fine mesopores (<10 nm) predominantly contribute to surface area development of the Eocene Bhainskati shales.

The N_2 physisorption isotherms exhibit notable hysteresis patterns ($P/P_0 > 0.5$) without a plateau at high pressure ($P/P_0 > 0.95$), suggesting the presence of both mesopores (resulting in hysteresis) and macropores (lack of plateau) according to IUPAC classification. The International Union of Pure and Applied Chemistry (IUPAC) provides six different types of isotherms and their interpretation to relate them with characteristics of the porous system (IUPAC, 1994; Thommes et al., 2015). The hysteresis in bulk shale samples indicates the predominance of mesopores, while mineral compositions, particularly clay minerals, contribute to the presence of macropores. Moreover, all isotherms show adsorption at shallow relative pressures ($P/P_0 < 0.01$), indicating the existence of micropores. Fig. 19(a)–(c) displays the N_2 adsorption isotherm for the samples examined in this study from the Eocene Bhainskati Formation, characterized by a reversed S-shaped curve, classified as type II curves, and sample LSS13 from Surkhet exhibits a Type I isotherm curve (Fig. 19(b)) according to BET classification. At relative pressures below 0.3, the adsorption volume gradually increases with pressure, showing a slightly convex curve indicating the transition from monomolecular to multimolecular layer adsorption. Between relative pressures of 0.3 and 0.8, the adsorption volume increases slowly, indicating a multilayer adsorption process. However, in the sample LSS1 from the Surkhet area, the adsorption volume increases relatively faster than the other shale samples and reaches more than 30 cm^3/gm@STP. When the relative pressure exceeds 0.8, there's a sudden, rapid increase in adsorption volume, suggesting the presence of large pores or fractures in the shale samples, facilitating significant N_2 influx. At the middle-pressure zone, the separation degree is highest.

The adsorption and desorption curves tend to overlap, indicating the development of conical and slit-shaped pores in the shales (Fig. 19). The pressure corresponding to the adsorption and desorption of the same pore is not the same, which causes the adsorption and desorption curves not to coincide. The adsorption-desorption curves for the Eocene shale samples from the Tansen and Surkhet areas differ because of the local tectonic activity. The pore structure characteristics can be determined according to the type of the desorption curve. This observation suggests that the gas adsorption and desorption within the same formation also have differences, mainly due to the different stages of tectonics from the collision to the evolution and post-evolution of the Himalayas. A few faults and thrusts are still active in the Himalayas, continuously impacting the structure of pores and gas accumulation and migration along the reservoir rocks.

5.3. Himalayan tectonic impact on rock strata, shale pore structure, gas accumulation, and preservation

The geological evolution driven by tectonic events significantly impacts shale formations, influencing their mechanical properties, fracture development, and gas preservation (Slatt and O'Brien, 2011). In the Tansen and Surkhet areas, the Eocene shale has been subjected to intense tectonic stress from the Himalayan Orogeny, resulting in NS-trending strike-slip faults, thrusts, and folds (Li et al., 2020). The collision of the Indian and Eurasian plates initiated episodic tectonic activity, beginning with the activation of the MCT at 23–18 Ma, which emplaced large thrust sheets (>100 km) and caused significant crustal thickening and deformation of the Lesser Himalayan Sequence (LHS) and Greater Himalayan Sequence (GHS) (DeCelles et al., 2020; Khanal et al., 2015). During the Late Miocene (11–5 Ma), deformation shifted to the Lesser Himalayan Duplex, accommodating ~12 km of slip and transitioning to subcritical taper (DeCelles et al., 2020). By the Pliocene–Pleistocene (<5 Ma), the MBT and frontal imbricate zone became active, concentrating shortening in the Siwalik Group foreland basin. The MBT, initially active at ~10 Ma, was reactivated at ~3 Ma, further eroding Lesser Himalayan rocks and exhuming the Himalayas (Khanal et al., 2015; Meigs et al., 1995). These tectonic processes created local-scale structures, such as anticlines and fault-bounded closures, which are critical for hydrocarbon accumulation (Mishra and Mukhopadhyay, 2012). The combined effects of these processes dictate the overall dynamics of the hydrocarbon system, affecting where and how hydrocarbon gases accumulate and are preserved within the Nepal Himalayas. The thrust faulting and duplexing in the Lesser and Sub-Himalayan zones create structural traps, such as anticlines and fault-bounded closures, which are critical for hydrocarbon accumulation (Mishra and Mukhopadhyay, 2012). While tectonic forces initially enhance porosity by generating fractures and pathways for fluid and gas migration, proximity to major faults (MCT, MBT) often increases tectonic stress, altering pore structures and reducing reservoir quality (Fan et al., 2022; Xiang et al., 2024). While tectonic deformation enhances macropore connectivity, it also impacts micropores and nanopores. In the Eocene shale of the Lesser Himalayan foreland basin, tectonic stress has led to the development of nanometer-sized pores (smaller than 4 nm), as evidenced by SEM image analysis, MICP, and gas adsorption data (Fig. 18(a)–(d)). These small pores, while beneficial for gas adsorption, pose challenges for gas flow due to high capillary pressure, especially in over-mature organic matter zones (Ma et al., 2014).

Tectonic deformation enhances the connectivity of pore networks (Zhu et al., 2018), while intense late tectonic reworking impacts shale gas diagenetic and preservation mechanisms,

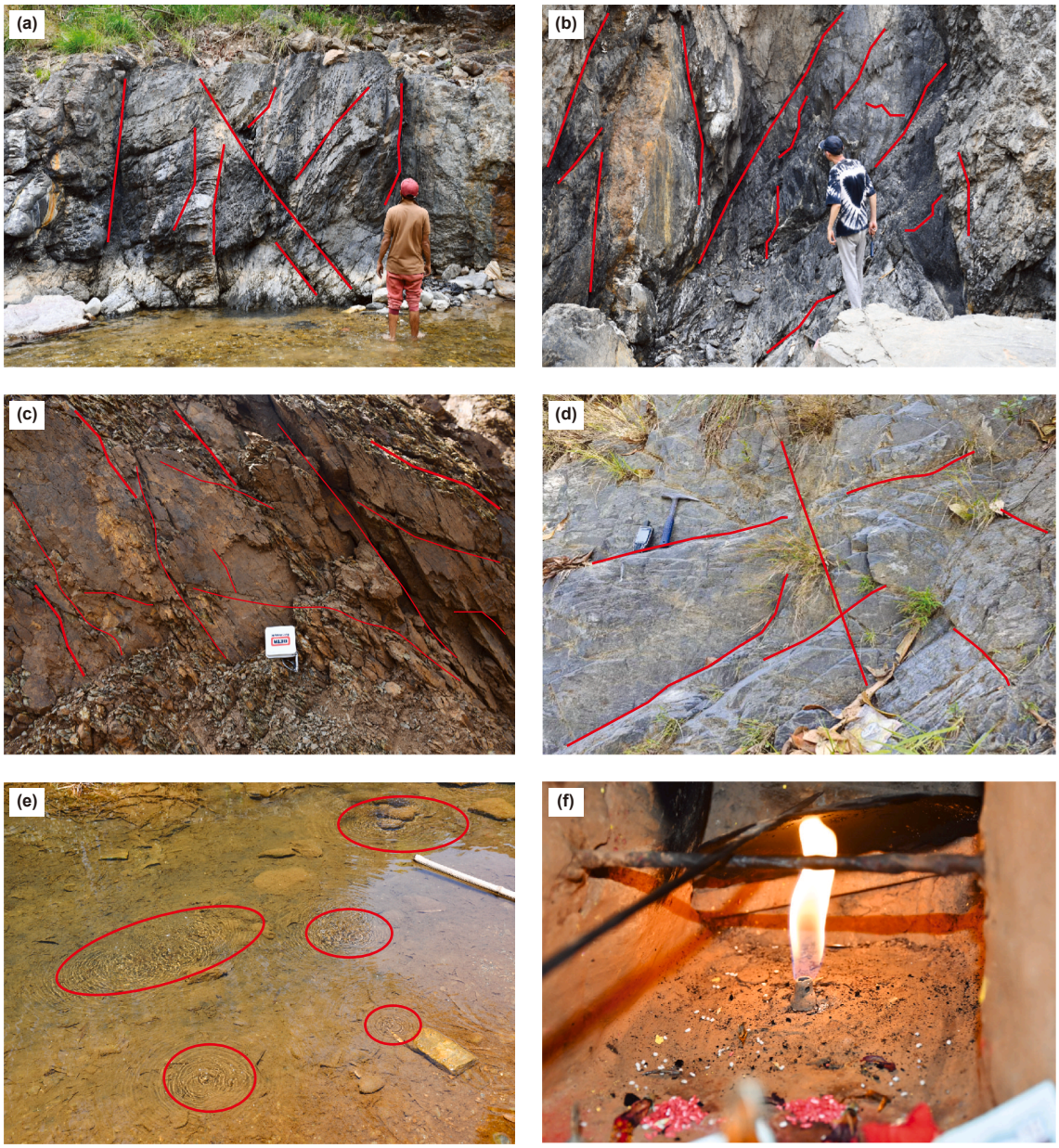

Fig. 20. Field photographs showing the outcrops and rocks of the Eocene shale in the study area. Bedding and joints in an outcrop shale of the (**a**)–(**b**) Tansen area with the impact of Pappa Klippe, (**c**)–(**d**) Surkhet area, (**e**) gas seepage evolves as bubbles in the Nabisthan river, and (**f**) gas burning flames near the river indicating gas seepage in the Dailekh area along the ridge of the anticline and Padukasthan Fault, north of Surkhet.

potentially leading to unfavorable conditions for shale gas preservation (Gou et al., 2021; Sun et al., 2023; Zhu et al., 2018). The impact of tectonic deformation on pore morphology may be either ductile deformation or brittle deformation. Tectonic deformation fundamentally alters the shale's pore structure, with ductile deformation resulting in a complete mixing of organic and clay minerals, forming the mylonite structure. In areas subjected to ductile deformation, such as the Palpa Klippe region (Figs. 2(a) and 20(a), (b)), the Eocene shale exhibits a mylonitic structure due to the complete mixing of organic matter and clay minerals. This process increases the SSA and enhances adsorption capacity, but it also reduces pore connectivity, particularly in nanopores (Ma et al., 2014). The dispersion of organic matter particles within clay minerals due to mylonitization further complicates the pore network, making gas flow more challenging. In contrast, brittle deformation, characterized by the development of fractures and joints, enhances macropore connectivity. The Eocene shale in the Tansen and Surkhet area displays diverse joint orientations and bedding plane crossings, accompanied by numerous fractures (Fig. 20). These intricate tectonic deformations can negatively impact shale gas reservoirs by allowing gas to escape through large open fractures, causing damage to the shale strata, floor, and sealing roof. Gas seepage in the Nabhisthan area along the Nabhisthan anticline and the Padhukasthan fault is proof of gas escaping from the faults in the sharp anticline (Fig. 20(e)–(f)). Proximity to faults results in stronger tectonic stress and deformation, adversely affecting porosity by altering the pore structure and reducing reservoir quality are negative impacts. Intense deformation and uplift typically reduce porosity by damaging the shale's pore structure (Fan et al., 2022; Xiang et al., 2024). Tectonic

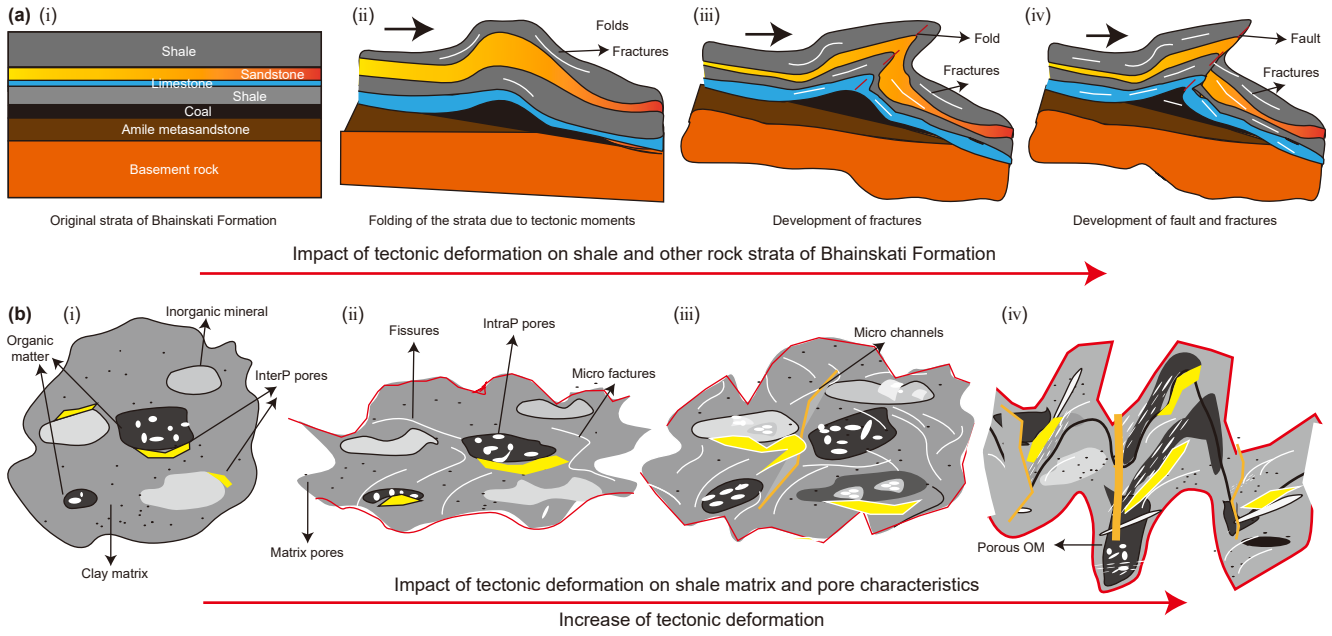

Fig. 21. Schematic model showing the possible effect of tectonic deformation on (**a**) the Bhainskati Formation rock strata and (**b**) the shale's pore structure development and deformation due to tectonism.

stress associated with Himalayan tectonic movements induces alterations in shale macromolecular structures, affecting gas adsorption and storage capacity (Feng et al., 2022; Guo et al., 2017). The continued tectonic deformation led to a complex pore network, vital for gas transport and storage but also prone to gas leakage (Han et al., 2022; Zhu et al., 2018). As the intensity of tectonic deformation superposition increased, the gas content in the shale gas gradually decreased (Hou et al., 2024).

The impact of tectonism on shale pore structure and gas preservation is evident through various stages of deformation, as depicted in the schematic cartoon model in Fig. 21. Shale gas production is stimulated by an enhanced seepage flow of gas adsorption and desorption when the small micro-fractures do not extend to the roof and floor of the shale strata, which preserves gases rather than allowing them to escape through the channel. Fig. 21(b) shows the possible pattern diagram of the development of the pore network in OM-clay aggregate shale during tectonic deformation. The development of micro-fractures with cement or veins can also contribute to the sealing ability of shale gas reservoirs, impeding free gas movement and enhancing preservation. However, intense tectonic deformation and uplift typically reduce porosity by damaging the shale's pore structure. Gas escapes through thrusts and faults, such as the Padukasthan fault, damages and enlarges shale structures, reducing the preservation capacity of pore spaces (Fan et al., 2022). The hydrocarbon generation leads to the formation of OM pores crucial for gas storage (Loucks et al., 2012). Gas production depends on natural fracture development, often influenced by tectonic events (Curtis, 2002). The tectonic stress during the dry gas generation stage leads to a notable decrease in organic pores and an increase in microfractures, following the pattern diagram of pore network development in OM-clay aggregate shale during tectonic deformation (Fig. 21(b)). Fault activity and sealing are crucial for the preservation of shale gas. Gas escapes through thrusts and faults, damages and enlarges shale structures, reducing the preservation capacity of pore spaces (Fan et al., 2022). While multi-stage and multi-oriented tectonic features facilitate the development of extensive fractures and fissures, they can also lead to gas leakage from the source and trap. The degree of pore development in the Eocene shale of the Tansen and Surkhet areas is strongly controlled by tectonic activity. While tectonic deformation enhances macropore connectivity and fracture development, it also damages the shale's pore structure, particularly in nanopores, reducing porosity and reservoir quality.

5.4. Comparative analysis with a similar complex tectonic setting

The Eocene Bhainskati Shale of the Lesser Himalaya, Nepal, is significantly impacted by the Himalayan tectonics, exhibiting similar characteristics comparable to other well-studied shale formations in the NW Himalayan region and SE China. The complex tectonics of the Northwest Himalayas significantly influence shale gas formation, accumulation, and preservation. The region's fold-and-thrust belt, shaped by the MBT and Main Central Thrust (MCT), creates various hydrocarbon traps like ramp anticlines and buried duplexes. Carbonaceous shale from the key formations, including the Patala and Nammal in Pakistan's Kohat-Potwar area and the Subathu and Lower Dharamsala in India, shows fair unconventional reservoirs (Craig et al., 2018; Hafiz et al., 2022; Khan et al., 2022; Mani et al., 2014), developed substantial hydrocarbon potential around 22-14 Ma, peaking in oil generation between 11 and 10 Ma during the establishment of the MBT (Craig et al., 2018). Structures formed approximately 6 Ma likely received gaseous hydrocarbons, while those linked to the 5 Ma MBT splay are prime targets for gas accumulation. The Subathu Formation extends from Pakistan's Potwar Basin to Nepal, varying in thickness from 50 to 1800 m due to tectonic complexity. The samples from Subathu Fm under SEM show abundant dispersed organic matter and are mainly composed of clay minerals with pyrite crystals (Hafiz et al., 2022). The Patala Shale is thermally less mature, whereas the Subathu and Bhainskati Shales are thermally overmature, possibly due to friction tectonics (Hafiz et al., 2022). These shales generally exhibit low to moderate porosity (2%–8%) and very low permeability, though natural fractures in the Patala and Subathu shales enhance permeability. The Patala Shale, located in the tectonically active Potwar Basin, is highly fractured, which enhances

permeability but poses risks to preservation (Khan et al., 2022). The highly thermally mature coal seams and carbonaceous shales, with low Hydrogen Index (HI), suggest deep burial and potential over-maturity from thrust tectonics. These Type III and IV kerogens generated gas in deeply buried subsurface areas over 6 km deep. The tectonic compression and uplift have enhanced gas generation by causing deep burial and increased thermal maturity, though they also lead to brittleness and frequent disruption of formations (Craig et al., 2018). This intense tectonic activity often breaches original traps, resulting in the loss of early-generated hydrocarbons. However, the Bhainskati Shale is more intensely deformed due to thrust faulting, which may compromise seal integrity while creating structural traps. Despite these challenges, the areas near the MBT and late-stage thrust structures remain promising for shale gas exploration, underscoring the dual role of Himalayan tectonism in facilitating and complicating hydrocarbon preservation in this research area.

In China, the Guizhou and Sichuan provinces, adjacent to the northern part of the Himalaya, exhibit the complex tectonic activities crucial in shale gas accumulation and preservation. These regions have experienced significant tectonic events, including the Yanshanian and Himalayan periods, resulting in well-developed faults and varied geological structures. In Guizhou, tectonic uplift, regional faults, strike-slip faults, and synclines facilitate gas migration to higher structural points, enhancing gas retention at greater burial depths despite reduced permeability. The Weiyuan and Zhaotong areas in Guizhou exhibit synclinal structures that act as natural traps for shale gas, with uplifted regions providing migration pathways for hydrocarbons (Sun et al., 2021). However, intense deformation in some areas can lead to permeability issues and gas dissipation, like the challenges faced in the Himalayan region. In contrast, the Sichuan Basin, influenced by multiple tectonic periods, displays variable preservation conditions. Anticlines in this region typically show higher gas enrichment than synclines due to better structural trapping. Favorable exploration targets include deep syncline cores and slopes with reverse faults, which provide effective seals for gas accumulation (Xiao et al., 2021). Samples from the Wufeng-Longmaxi Formation in the Xiushan region exhibit varying deformation strengths, with increasing deformation leading to a gradual reduction in micropores and a corresponding increase in macropores (Li et al., 2021). The Longmaxi Formation in Sichuan, for instance, benefits from less intense deformation compared to the Himalayan region, enabling large-scale commercial production through hydraulic fracturing. The tectonic stress and structural deformation in the Wufeng-Longmaxi formations of the southeastern Sichuan Basin, Yongshun, influence pore surface area and adsorption capacity by compressing mesopores and generating macropores through microcrack development. At the same time, total porosity and micropores remain relatively constant (Liang et al., 2017). The intense tectonism in the Himalayan region, characterized by thrust faults, folds, and uplift, has a similar impact on shale gas reservoirs as observed in Guizhou and Sichuan. The Eocene Bhainskati Shale in the Nepalese Lesser Himalayas experiences significant deformation, which enhances gas adsorption but often leads to permeability challenges and gas escape through fractures and faults. This mirrors the tectonic uplift in Guizhou, where gas migration is facilitated, but preservation is compromised in highly deformed zones. Furthermore, in Sichuan, the complex tectonic history, including the influence of Himalayan orogeny, creates mixed preservation outcomes. The interplay between compression and uplift in the Himalayan foreland basin is analogous to the tectonic dynamics in Sichuan, where anticlines and reverse faults play a critical role in gas enrichment. The Himalayan thrust systems, such as the MCT and the MBT, create structural traps similar to those in Sichuan, where fault-bounded closures and anticlines are key to hydrocarbon accumulation. Regarding organic matter and thermal maturity, both regions exhibit high organic matter content and thermal maturity, which are essential for shale gas generation. In Guizhou, the Lower Silurian Longmaxi Formation is rich in organic matter, with thermal maturity levels conducive to gas generation (Sun et al., 2021). In Sichuan, the Longmaxi Formation benefits from optimal thermal maturity and less intense deformation (Xiao et al., 2021), allowing for effective gas retention and production. The Himalayan tectonism, however, often pushes organically rich Eocene Bhainskati shale formations to higher maturity levels, increasing gas generation but also risking gas escape through fractures and faults. The structural complexity is driven by Himalayan tectonism, which influences gas preservation. In Guizhou, synclines and faults create natural traps, but intense deformation can lead to gas dissipation. In Sichuan, anticlines and reverse faults provide favorable conditions for gas accumulation, but variable tectonic stress can compromise preservation in some areas (Xiao et al., 2021). The tectonic activities in the Sichuan and Guizhou regions, influenced by Himalayan tectonism, provide valuable analogs for understanding shale gas accumulation and preservation in the Eocene shales of the Nepalese Lesser Himalayas.

6. Conclusion

This study comprehensively characterizes the pore structure of shale from the Eocene Bhainskati Formation within the Lesser Himalayas, revealing the impacts of tectonism, mineralogy, and thermal maturity. Furthermore, it offers valuable insights into the pore structure and distribution of highly matured and tectonically deformed shales, providing implications for understanding gas reservoir behavior and optimizing shale gas exploration and extraction strategies.

1. SEM analysis reveals the presence of OM hosted pores, mineral matrix pores (InterP, IntraP), and organic pores with microfractures exhibiting apertures exceeding 100 nm to 1 μm in size in the Eocene Bhainskati shales. The plot between TOC and porosity in the Eocene shales does not show a direct correlation. However, thermal maturity negatively impacts specific surface area, pore volume, pore diameter, and porosity. Low TOC levels and over-maturity are associated with extensive tectonic activities in the Himalayan Orogeny.
2. The specific surface area of the shale samples ranges from 24.34 to 29.93 m^2/g, with BJH pore volume varying between 0.0855 and 0.1297 cm^3/g. Tectonic activity raises the pores' SSA, enhancing their tectonically deformed shale adsorption capability. Tectonic deformation alters shale pore structure by shifting from brittle to ductile deformation, leading to changes in pore size distribution and connectivity.
3. MICP and gas adsorption methods identify the presence of all three types of pores in the Eocene Bhainskati shale, with a higher proportion of mesopores than the others. Based on surface area, micropores constitute 48.01%–51.83%, mesopores 44.39%–51.27%, and macropores 0.71%–3.78%. Meanwhile, based on pore volume, micropores represent 16.91%–20.72%, mesopores 30.24%–64.07%, and macropores 17.30%–49.34%. The analysis reveals significant pore volumes and surface area variation within the same rock strata.
4. The Eocene Bhainskati shale is a composite reservoir system whose character is fundamentally shaped by its tectonic history. While thermal maturity generated gas by creating isolated organic nanopores for adsorption, the intense tectonic compression of the Himalayan foreland basin dictated the final pore architecture. This deformation plays a dual role: it destructively collapses and reshapes organic porosity yet

constructively enhances the reservoir's permeability by generating a pervasive, propped network of microfractures. Consequently, the capacity for gas storage and migration is not solely a function of organic content. Still, it is governed by the tectonically modified pore system, where fractures provide the critical pathways for gas flow.

5. The Himalayan tectonic forces, including regional thrusts such as MCT, MBT, and RMT, alongside local features like the Palpa Klippe in the Tansen area, impact the Eocene source rock and the sealing behavior of overlying shale. These tectonic activities significantly influence shale gas preservation and gas dynamics by altering pore structures, promoting the escape of gases along the faults and ridge of folds. Understanding the impact of tectonic activity on shale deformation is vital for assessing shale gas potential and optimizing exploration strategies in tectonically active Himalayan regions.
6. The Eocene shale within the Lesser Himalayas, characterized by complex tectonics like those in the Northwest Himalayas and Southern China adjacent to the Himalayas, reveals significant impacts in shale gas formation, accumulation, and preservation. Tectonic forces such as thrusting and multiple uplift events enhance gas retention by altering pore structures. However, they also pose challenges, such as gas dissipation and reduced permeability. These findings highlight the dual impact of tectonic activity, which both facilitates and complicates the potential for shale gas across various geologically active zones.
7. This study provides a foundational characterization of the Bhainskati shale's pore system; however, its findings are constrained by the inherent limitations of outcrop-based analysis. The reliance on surface samples means that the petrophysical properties measured are likely to differ from those *in situ*, and the absence of direct gas content measurements prevents a definitive assessment of net gas retention versus tectonic escape. Consequently, these conclusions underscore the need for future subsurface validation through drilling and core-based studies to accurately quantify shale gas potential and the impacts of the Himalayan tectonics on shale's pore structure.

CRediT authorship contribution statement

Kumar Khadka: Writing – review & editing, Writing – original draft, Visualization, Software, Methodology, Investigation, Formal analysis, Data curation, Conceptualization. **Si-Jie Han:** Writing – review & editing, Validation, Project administration, Methodology. **Shu-Xun Sang:** Writing – review & editing, Visualization, Supervision, Resources, Funding acquisition, Conceptualization. **Jun-Jie He:** Software, Resources, Investigation, Formal analysis, Data curation. **Upendra Baral:** Writing – review & editing, Visualization, Validation, Resources, Investigation. **Saunak Bhandari:** Writing – review & editing, Visualization, Software, Investigation. **Debashish Mondal:** Writing – review & editing, Software. **Xiao-Zhi Zhou:** Writing – review & editing, Visualization. **Shi-Qi Liu:** Writing – review & editing, Visualization.

Data availability statement

Not applicable.

Declaration of competing interest

The authors declare that they have no known competing financial interests or personal relationships that could have appeared to influence the work reported in this paper.

Acknowledgments

This work was financially supported by the "Belt and Road" Innovation Cooperation Project of Jiangsu Province (Grant No. BZ2022015) and the National Natural Science Foundation of China (No. 42030810). Author U. Baral is partially supported by the International Partnership Program of the Chinese Academy of Sciences (Grant/Award Number: 131551KYSB20200021). We also acknowledge the Department of Mines and Geology, Nepal, for geological fieldwork permission and sample shipping.

References

Aringhieri, R., 2004. Nanoporosity characteristics of some natural clay minerals and soils. Clays Clay Miner. 52 (6), 700–704. https://doi.org/10.1346/CCMN.2004.0520604.

Bai, B., Wang, G., Shang, F., Zhou, H., Liu, Y., Shi, Z., 2024. Effects of SEM image resolution on organic pore structure estimation of shale reservoirs. Gas Sci. Eng. 121, 205170. https://doi.org/10.1016/j.jgsce.2023.205170.

Chalmers, G.R., Bustin, R.M., Power, I.M., 2012. Characterization of gas shale pore systems by porosimetry, pycnometry, surface area, and field emission scanning electron microscopy/transmission electron microscopy image analyses: examples from the Barnett, Woodford, Haynesville, Marcellus, and Doig units. AAPG Bull. 96 (6), 1099–1119. https://doi.org/10.1306/10171111052.

Chalmers, G.R.L., Bustin, R.M., 2007. The organic matter distribution and methane capacity of the Lower Cretaceous strata of Northeastern British Columbia, Canada. Int. J. Coal Geol. 70 (1), 223–239. https://doi.org/10.1016/j.coal.2006.05.001.

Chen, S., Gong, Z., Li, X., Wang, H., Wang, Y., Zhang, Y., 2021. Pore structure and heterogeneity of shale gas reservoirs and its effect on gas storage capacity in the Qiongzhusi Formation. Geosci. Front. 12 (6), 101244. https://doi.org/10.1016/j.gsf.2021.101244.

Chen, Y., Tang, S., Tang, H., Xi, Z., Zhao, N., Sun, S., Zhou, T., Zhao, S., 2024. Pore structure heterogeneity of deep marine shale in complex tectonic zones and its implications for shale gas exploration. Energy Fuel 38 (3), 1891–1905. https://doi.org/10.1021/acs.energyfuels.3c03882.

Clarkson, C.R., Solano, N., Bustin, R.M., Bustin, A.M.M., Chalmers, G.R.L., He, L., Melnichenko, Y.B., Radliński, A.P., Blach, T.P., 2013. Pore structure characterization of North American shale gas reservoirs using USANS/SANS, gas adsorption, and mercury intrusion. Fuel 103, 606. https://doi.org/10.1016/j.fuel.2012.06.119.

Craig, J., Hakhoo, N., Bhat, G.M., Hafiz, M., Khan, M.R., Misra, R., Pandita, S.K., Raina, B.K., Thurow, J., Thusu, B., Ahmed, W., Khullar, S., 2018. Petroleum systems and hydrocarbon potential of the North-West Himalaya of India and Pakistan. Earth Sci. Rev. 187, 109–185. https://doi.org/10.1016/j.earscirev.2018.09.012.

Curtis, J.B., 2002. Fractured shale-gas systems. AAPG (Am. Assoc. Pet. Geol.) Bull. 86 (11), 1921–1938. https://doi.org/10.1306/61eeddbe-173e-11d7-8645000102c1865d.

Curtis, M.E., Cardott, B.J., Sondergeld, C.H., Rai, C.S., 2012. Development of organic porosity in the Woodford Shale with increasing thermal maturity. Int. J. Coal Geol. 103, 26–31. https://doi.org/10.1016/j.coal.2012.08.004.

Decelles, P.G., 2012. Foreland basin systems revisited: variations in response to tectonic settings. In: Busby, C., Azor, A. (Eds.), Tectonics of Sedimentary Basins: Recent Advances, first ed. Blackwell Publishing Ltd.

DeCelles, P.G., Carrapa, B., Ojha, T.P., Gehrels, G.E., Collins, D., 2020. Structural and thermal evolution of the Himalayan thrust Belt in midwestern Nepal. Struct. Therm. Evol. Himalayan Thrust Belt Midwestern Nepal 547, 1–79. https://doi.org/10.1130/2020.2547(01).

DeCelles, P.G., Gehrels, G.E., Najman, Y., Martin, A.J., Carter, A., Garzanti, E., 2004. Detrital geochronology and geochemistry of cretaceous–early Miocene strata of Nepal: Implications for timing and diachroneity of initial Himalayan orogenesis. Earth Planet Sci. Lett. 227 (3–4), 313–330. https://doi.org/10.1016/j.epsl.2004.08.019.

DeCelles, P.G., Gehrels, G.E., Quade, J., Ojha, T.P., 1998. Eocene-early Miocene foreland basin development and the history of Himalayan thrusting, western and central Nepal. Tectonics 17 (5), 741–765. https://doi.org/10.1029/98tc02598.

Dhital, M., 2015. Geology of the Nepal Himalaya, vol. 1. Springer. https://doi.org/10.1007/978-3-319-02496-7.

Fan, C., Xie, H., Li, H., Zhao, S., Shi, X., Liu, J., Meng, L., Hu, J., Lian, C., 2022. Complicated fault characterization and its influence on shale gas preservation in the Southern Margin of the Sichuan Basin, China. Lithosphere 2022 (Special 12), 8035106. https://doi.org/10.2113/2022/8035106.

Feng, Q., Qiu, N., Borjigin, T., Wu, H., Zhang, J., Shen, B., Wang, J., 2022. Tectonic evolution revealed by thermo-kinematic and its effect on shale gas preservation. Energy 240, 122781. https://doi.org/10.1016/j.energy.2021.122781.

Gao, J., Li, X., Cheng, G., Luo, H., Zhu, H., 2023. Structural evolution and characterization of organic-rich shale from macroscopic to microscopic resolution: The significance of tectonic activity. Adv. Geo-Energy Res. 10 (2), 84–90. https://doi.org/10.46690/ager.2023.11.03.

Ghanizadeh, A., Clarkson, C.R., Aquino, S., Ardakani, O.H., Sanei, H., 2015. Petrophysical and geomechanical characteristics of Canadian tight oil and liquid-rich gas reservoirs: I. Pore network and permeability characterization. Fuel 153, 664–681. https://doi.org/10.1016/j.fuel.2015.03.020.

Gou, Q., Xu, S., Hao, F., Yang, F., Shu, Z., Liu, R., 2021. The effect of tectonic deformation and preservation condition on the shale pore structure using adsorption-based textural quantification and 3D image observation. Energy 219, 119579. https://doi.org/10.1016/j.energy.2020.119579.

Guo, T., 2016. Key geological issues and main controls on accumulation and enrichment of Chinese shale gas. Petrol. Explor. Dev. 43 (3), 349–359. https://doi.org/10.1016/S1876-3804(16)30042-8.

Guo, X., Hu, D., Li, Y., Wei, Z., Wei, X., Liu, Z., 2017. Geological factors controlling shale gas enrichment and high production in Fuling shale gas field. Petrol. Explor. Dev. 44 (4), 513–523. https://doi.org/10.1016/S1876-3804(17)30060-5.

Hafiz, M., Hakhoo, N., Bhat, G., Kanungo, S., Thusu, B., Craig, J., Ahmed, W., Magotra, R., 2022. An assessment of the source potential and reservoir characterization for tight gas exploration in the Subathu Formation shale, Himalayan Foreland Basin, Northwestern India. J. Asian Earth Sci. 230, 105205. https://doi.org/10.1016/j.jseaes.2022.105205.

Han, M.L., Wei, X.L., Zhang, J.C., Liu, Y., Tang, X., Li, P., Liu, Z.Y., 2022. Influence of structural damage on evaluation of microscopic pore structure in marine continental transitional shale of the Southern North China Basin: A method based on the low-temperature N_2 adsorption experiment. Pet. Sci. 19 (1), 100–115. https://doi.org/10.1016/j.petsci.2021.10.016.

Hou, H., Yang, W., Du, W., Feng, X., Jiang, Z., Shi, F., Lin, R., Wang, Y., Zhang, D., Chen, Y., Sun, Z., Zhao, F., 2024. Implications of multi-stage deformation on the differential preservation of lower Paleozoic shale gas in tectonically complex regions: New structural and kinematic constraints from the Upper Yangtze Platform, South China. Mar. Petrol. Geol. 160, 106629. https://doi.org/10.1016/j.marpetgeo.2023.106629.

IUPAC, 1994. Characterization of Porous Solids: Recommendations for the Characterization of Porous Solids. Pure and Applied Chemistry, 66 (8).

Jarvie, D.M., Hill, R.J., Ruble, T.E., Pollastro, R.M., 2007. Unconventional shale-gas systems: The Mississippian Barnett Shale of north-central Texas as one model for thermogenic shale-gas assessment. AAPG Bull. 91 (4), 475–499. https://doi.org/10.1306/12190606068.

Josh, M., Esteban, L., Delle Piane, C., Sarout, J., Dewhurst, D.N., Clennell, M.B., 2012. Laboratory characterisation of shale properties. J. Petrol. Sci. Eng. 88–89, 107–124. https://doi.org/10.1016/j.petrol.2012.01.023.

Ju, Y., Sun, Y., Tan, J., Bu, H., Han, K., Li, X., Fang, L., 2018. The composition, pore structure characterization and deformation mechanism of coal-bearing shales from tectonically altered coalfields in Eastern China. Fuel 234, 626–642. https://doi.org/10.1016/j.fuel.2018.06.116.

Khadka, K., Sang, S., Han, S., He, J., Baral, U., Bhandari, S., 2024. Geological and geochemical characterisation of shale as an unconventional gas source and reservoir within the Lesser Himalaya, Nepal. Geological Journal. https://doi.org/10.1002/gj.5112, 60(4), 923-941.

Khadka, K., Sang, S., Han, S., He, J., Baral, U., Bhandari, S., Mondal, D., 2025. Geochemical and mineralogical insights into organic matter preservation in the Gondwana and post-Gondwana shale of the Lesser Himalayas, Nepal. Minerals 15 (1), 63. https://doi.org/10.3390/min15010063.

Khan, N., Weltje, G.J., Jan, I.U., Swennen, R., 2022. Depositional and diagenetic constraints on the quality of shale-gas reservoirs: A case study from the late Palaeocene of the Potwar Basin (Pakistan, Eastern Tethys). Geol. J. 57, 2770–2787.. https://doi.org/10.1002/gj.4439.

Khanal, S., Robinson, D.M., Kohn, M.J., Mandal, S., 2015. Evidence for a far-traveled thrust sheet in the Greater Himalayan thrust system, and an alternative model to building the Himalaya. Tectonics 34 (1), 31–52. https://doi.org/10.1002/2014tc003616.

Li, S., Li, Y., He, Z., Chen, K., Zhou, Y., Yan, D., 2020. Differential deformation on two sides of Qiyueshan Fault along the eastern margin of Sichuan Basin, China, and its influence on shale gas preservation. Mar. Petrol. Geol. 121, 104602. https://doi.org/10.1016/j.marpetgeo.2020.104602.

Li, X., Zhu, H., Zhang, K., Li, Z., Yu, Y., Feng, X., Wang, Z., 2021. Pore characteristics and pore structure deformation evolution of ductile deformed shales in the Wufeng-Longmaxi Formation, southern China. Mar. Petrol. Geol. 127, 104992. https://doi.org/10.1016/j.marpetgeo.2021.104992.

Li, Z., Li, Q., Zhang, D., Tan, F., Rajaure, S., Zhao, G., Tripathi, G.N., Du, B., Yang, P., 2022. Seismic Survey in lesser Himalayan Thrust Belt, Western Nepal. Int. J. Geophys. 2022, 8026088. https://doi.org/10.1155/2022/8026088.

Liang, M., Wang, Z., Gao, L., Li, C., Li, H., 2017. Evolution of pore structure in gas shale related to structural deformation. Fuel 197, 310–319. https://doi.org/10.1016/j.fuel.2017.02.035.

Liu, X., Xiong, J., Liang, L., 2015. Investigation of pore structure and fractal characteristics of organic-rich Yanchang Formation shale in central China by nitrogen adsorption/desorption analysis. J. Nat. Gas Sci. Eng. 22, 62–72. https://doi.org/10.1016/j.jngse.2014.11.020.

Loucks, R.G., Reed, R.M., Ruppel, S.C., Hammes, U., 2012. Spectrum of pore types and networks in mudrocks and a descriptive classification for matrix-related mudrock pores. AAPG (Am. Assoc. Pet. Geol.) Bull. 96, 1071–1098. https://doi.org/10.1306/08171111061.

Loucks, R.G., Reed, R.M., Ruppel, S.C., Jarvie, D.M., 2009. Morphology, Genesis, and distribution of nanometer-scale pores in siliceous mudstones of the Mississippian Barnett shale. J. Sediment. Res. 79 (12), 848–861. https://doi.org/10.2110/jsr.2009.092.

Ma, K., Zhang, B., Wen, S., Lin, X., Wang, Y., Yang, K., 2022. Quantitative characterization and controlling factors of shallow shale Reservoir in Taiyang Anticline, Zhaotong area, China. Minerals 12 (8), 998. https://www.mdpi.com/2075-163X/12/8/998.

Ma, Y., Zhong, N., Han, H., Li, D., Zhang, Y., Cheng, L., 2014. Definition and structure characteristics of pores in mylonitized organic-rich shales. Sci. China Earth Sci. 57 (12), 3027–3034. https://doi.org/10.1007/s11430-014-4968-3.

Mani, D., Patil, D.J., Dayal, A.M., Kavitha, S., Hafiz, M., Hakhoo, N., Bhat, G.M., 2014. Gas potential of Proterozoic and Phanerozoic shales from the NW Himalaya, India: Inferences from pyrolysis. Int. J. Coal Geol. 128–129, 81–95. https://doi.org/10.1016/j.coal.2014.04.007.

Mastalerz, M., Drobniak, A., Stankiewicz, A.B., 2018. Origin, properties, and implications of solid bitumen in source-rock reservoirs: A review. Int. J. Coal Geol. 195, 14–36. https://doi.org/10.1016/j.coal.2018.05.013.

Medina-Rodriguez, B.X., Alvarado, V., 2021. Use of gas adsorption and inversion methods for shale pore structure characterization. Energies 14 (10), 2880. https://www.mdpi.com/1996-1073/14/10/2880.

Meigs, A.J., Burbank, D.W., Beck, R.A., 1995. Middle-late Miocene (>10 Ma) formation of the Main Boundary thrust in the western Himalaya. Geology 23 (5), 423–426. https://doi.org/10.1130/0091-7613(1995)023<0423:MLMMFO>2.3.CO;2.

Milliken, K.L., Rudnicki, M., Awwiller, D.N., Zhang, T., 2013. Organic matter-hosted pore system, Marcellus Formation (Devonian), Pennsylvania. AAPG (Am. Assoc. Pet. Geol.) Bull. 97 (2), 177–200. https://doi.org/10.1306/07231212048.

Mishra, P., Mukhopadhyay, D.K., 2012. Structural evolution of the frontal fold–thrust belt, NW Himalayas from sequential restoration of balanced cross-sections and its hydrocarbon potential. Geol. Soc. 366 (1), 201–228. https://doi.org/10.1144/sp366.6.

Morley, C.K., von Hagke, C., Hansberry, R.L., Collins, A.S., Kanitpanyacharoen, W., King, R., 2017. Review of major shale-dominated detachment and thrust characteristics in the diagenetic zone: Part I, meso- and macro-scopic scale. Earth Sci. Rev. 173, 168–228. https://doi.org/10.1016/j.earscirev.2017.07.019.

Ping, Y., Fuwen, T., Meifeng, S., Zhenghe, W., Zhongxiong, L., Wangzhong, Z., Rajaure, S., Tripathi, G.N., 2021. Oil- source correlation and hydrocarbon accumulation in the Lesser Himalayan belt of Nepal. Acta Geol. Sin. 95 (11), 3426–3441. https://doi.org/10.19762/j.cnki.dizhixuebao.2021179 (in Chinese).

Qian, Y., Gao, P., Fang, X., Sun, F., Cai, Y., Zhou, Y., 2022. Microstructure characterization techniques for shale reservoirs: A review. Front. Earth Sci. 10. https://doi.org/10.3389/feart.2022.930474.

Robinson, D.M., DeCelles, P.G., Copeland, P., 2006. Tectonic evolution of the Himalayan thrust belt in western Nepal: implications for channel flow models. Geol. Soc. Am. Bull. 118 (7–8), 865–885. https://doi.org/10.1130/b25911.1.

Robinson, D.M., DeCelles, P.G., Patchett, P.J., Garzione, C.N., 2001. The kinematic evolution of the Nepalese Himalaya interpreted from Nd isotopes. Earth Planet Sci. Lett. 192, 507–521. https://doi.org/10.1016/S0012-821X(01)00451-4.

Ross, D.J.K., Marc Bustin, R., 2009. The importance of shale composition and pore structure upon gas storage potential of shale gas reservoirs. Mar. Petrol. Geol. 26 (6), 916–927. https://doi.org/10.1016/j.marpetgeo.2008.06.004.

Sakai, 1983. Geology of the Tansen Group of the Lesser Himalaya in Nepal, vol. 25. Memoirs of the Faculty of Science Kyushu University Series D Geology, pp. 27–74. https://doi.org/10.5109/1546083.

Shang, X., Long, S., Duan, T., 2021. Fracture system in shale gas reservoir: prospect of characterization and modeling techniques. J. Nat. Gas Geosci. 6 (3), 157–172. https://doi.org/10.1016/j.jnggs.2021.06.001.

Sing, K., 2001. The use of nitrogen adsorption for the characterisation of porous materials. Colloids Surf. A Physicochem. Eng. Asp. 187–188, 3–9. https://doi.org/10.1016/S0927-7757(01)00612-4.

Singh, B.P., Singh, Y.R., Andotra, D.S., Patra, A., Srivastava, V.K., Guruaribam, V., Sijagurumayum, U., Singh, G.P., 2016. Tectonically driven late Paleocene (57.9–54.7 Ma) transgression and climatically forced latest middle Eocene (41.3–38.0 Ma) regression on the Indian subcontinent. J. Asian Earth Sci. 115, 124–132. https://doi.org/10.1016/j.jseaes.2015.09.030.

Slatt, R.M., O'Brien, N.R., 2011. Pore types in the Barnett and Woodford gas shales: Contribution to understanding gas storage and migration pathways in fine-grained rocks. AAPG Bull. 95 (12), 2017–2030. https://doi.org/10.1306/03301110145.

Sun, C., Nie, H., Dang, W., Chen, Q., Zhang, G., Li, W., Lu, Z., 2021. Shale gas exploration and development in China: Current status, geological challenges, and future directions. Energy Fuel 35 (8), 6359–6379. https://doi.org/10.1021/acs.energyfuels.0c04131.

Sun, M., Zhao, J., Pan, Z., Hu, Q., Yu, B., Tan, Y., Sun, L., Bai, L., Wu, C., Blach, T.P., Zhang, Y., Zhang, C., Cheng, G., 2020. Pore characterization of shales: A review of small angle scattering technique. J. Nat. Gas Sci. Eng. 78, 103294. https://doi.org/10.1016/j.jngse.2020.103294.

Sun, W., Zuo, Y., Lin, Z., Wu, Z., Liu, H., Lin, J., Chen, B., Chen, Q., Pan, C., Lan, B., Liu, S., 2023. Impact of tectonic deformation on shale pore structure using adsorption experiments and 3D digital core observation: A case study of the Niutitang Formation in Northern Guizhou. Energy 278, 127724. https://doi.org/10.1016/j.energy.2023.127724.

Sun, W., Zuo, Y., Wu, Z., Liu, H., Zheng, L., Wang, H., Shui, Y., Lou, Y., Xi, S., Li, T., Luo, X., 2020. Pore characteristics and evolution mechanism of shale in a complex tectonic area: Case study of the Lower Cambrian Niutitang Formation in Northern Guizhou, Southwest China. J. Petrol. Sci. Eng. 193, 107373. https://doi.org/10.1016/j.petrol.2020.107373.

Thommes, M., Kaneko, K., Neimark, A.V., Olivier, J.P., Rodriguez-Reinoso, F., Rouquerol, J., Sing, K.S.W., 2015. Physisorption of gases, with special reference

to the evaluation of surface area and pore size distribution (IUPAC Technical report). Pure Appl. Chem. 87 (9–10), 1051–1069. https://doi.org/10.1515/pac-2014-1117.

Wang, Y., Wang, Z., Zhang, Z., Yao, S., Zhang, H., Zheng, G., Luo, F., Feng, L., Liu, K., Jiang, L., 2024. Recent techniques on analyses and characterizations of shale gas and oil reservoir. Energy Rev. 3 (2), 100067. https://doi.org/10.1016/j.enrev.2023.100067.

Wang, Z., Tan, F., Sudhir, R., Ganesh, N.T., Du, B., Yang, P., 2022. The tectonosedimentary evolution since Proterozoic in Nepal and its Southern adjacent areas. Earth Sci. J. China Univ. Geosci. 47 (2), 405–417. https://doi.org/10.3799/dqkx.2021.087 (in Chinese).

Wang, Z.H., W, T.F., W, D.B., P, Y., Sudhir, R., Nath, T.G., 2023. Basic Petroleum geological conditions in Nepal and its implications for hydrocarbon exploration. Geol. Bull. China 42 (Z1), 411–419. https://kns.cnki.net/kcms/detail/11.4648.P.20221111.1508.004.html.

Xiang, M., Xu, S., We, Y.R., Gou, Q.Y., Li, B.C., 2024. Influence of tectonic preservation conditions on the nanopore structure of shale reservoir: A case study of Wufeng-Longmaxi Formation shale in western Hubei area, South China. Pet. Sci. https://doi.org/10.1016/j.petsci.2024.02.008.

Xiao, D., Wen, L., Zhang, Y., Xie, C., Tan, X., Cao, J., 2021. Natural gas accumulation in the basin–mountain transition zone, northwestern Sichuan Basin, China. Mar. Petrol. Geol. https://doi.org/10.1016/j.marpetgeo.2021.105305.

Xiong, F., Jiang, Z., Li, P., Wang, X., Bi, H., Li, Y., Wang, Z., Amooie, M.A., Soltanian, M.R., Moortgat, J., 2017. Pore structure of transitional shales in the Ordos Basin, NW China: Effects of composition on gas storage capacity. Fuel 206, 504–515. https://doi.org/10.1016/j.fuel.2017.05.083.

Xu, R., Prodanović, M., 2018. Effect of pore geometry on nitrogen sorption isotherms interpretation: A pore network modeling study. Fuel 225, 243–255. https://doi.org/10.1016/j.fuel.2018.03.143.

Xu, Z., Shi, W., Zhai, G., Peng, N., Zhang, C., 2020. Study on the characterization of pore structure and main controlling factors of pore development in gas shale. J. Nat. Gas Geosci. 5 (5), 255–271. https://doi.org/10.1016/j.jnggs.2020.09.003.

Yang, P., Tan, F., Shi, M., Wang, Z., Li, Z., Zhan, W., Rajaure, S., Tripathi, G.N., 2021. Oil-source correlation and hydrocarbon accumulation in the Lesser Himalayan belt of Nepal. Acta Geol. Sin. 95 (11), 3426–3441. https://doi.org/10.19762/j.cnki.dizhixuebao.2021179 (in Chinese).

Yin, T., Liu, D., Cai, Y., Zhou, Y., 2019. Methane adsorption constrained by pore structure in high-rank coals using FESEM, CO_2 adsorption, and NMRC techniques. Energy Sci. Eng. 7 (1), 255–271. https://doi.org/10.1002/ese3.275.

Zeng, L., Zhu, H., Hao, Y., Shi, E., Lu, Y., Qi, Y., 2023. Microstructures and pore structures of naturally deformed shales: Significance for shale gas exploration in the complex tectonic areas of the Margin of the Sichuan Basin, south China. Energy Fuel 37 (14), 10414–10425. https://doi.org/10.1021/acs.energyfuels.3c01539.

Zhang, T., Ellis, G.S., Ruppel, S.C., Milliken, K., Yang, R., 2012. Effect of organic-matter type and thermal maturity on methane adsorption in shale-gas systems. Org. Geochem. 47, 120–131. https://doi.org/10.1016/j.orggeochem.2012.03.012.

Zhang, Y., Yu, B., Pan, Z., Hou, C., Zuo, Q., Sun, M., 2020. Effect of thermal maturity on shale pore structure: A combined study using extracted organic matter and bulk shale from Sichuan Basin, China. J. Nat. Gas Sci. Eng. 74, 103089. https://doi.org/10.1016/j.jngse.2019.103089.

Zhu, H., Ju, Y., Qi, Y., Huang, C., Zhang, L., 2018. Impact of tectonism on pore type and pore structure evolution in organic-rich shale: Implications for gas storage and migration pathways in naturally deformed rocks. Fuel 228, 272–289. https://doi.org/10.1016/j.fuel.2018.04.137.